의 학 박 사 학 위 논 문

Development of a multimodal imaging agent for sentinel lymph node mapping using ^{99m}Tc-labeled mannosylated human serum albumin and dye conjugates

^{99m}Tc-MSA와 염료 접합체를 사용한 감시림프절 맵핑용 다중모드영상제의 개발

2019년 2월

서울대학교 대학원

의과학과 의과학전공

이 지 연

ABSTRACT

Development of a multimodal imaging agent for sentinel lymph node mapping using ^{99m}Tc-labeled mannosylated human serum albumin and dye conjugates

Ji Youn Lee

Departments of Biomedical Sciences,

Seoul National University Graduate School,

Seoul National University

Purpose:

Sentinel lymph node (SLN) is the first regional lymph node (LN) existing

nearest to the primary tumor. The detection of SLN in breast cancer and melanoma patients is important to evaluate tumor staging or to establish therapeutic decision-making. Blue dyes, radiotracers, combination of a radiotracer and blue dye method and radiolabeled blue dyes have been clinically used for SLN detection. However, these methods still have some limitations.

Here, the aim for this study was to develop a SLN mapping agent using ^{99m}Tc-labeled mannosylated human serum albumin (MSA) and dyes. Various dyes were tested by in vitro experiments such as binding efficiency with MSA, size exclusion liquid chromatography with HPLC and fluorescent screening. The selected dye, naphthol blue black (NBB) which showed the highest binding efficiency with MSA, was tested regarding its ability for SLN mapping by visual investigation, fluorescence imaging, and single photon emission computed tomography (SPECT)/computed tomography (CT).

Methods:

Visible screening was performed using 8 different dyes. Each 1 mM dye solution was prepared by dissolving 1 μmol of dye in 1 mL of distilled water (DW) and the solution was serially diluted from 0.25 to 0.001 mM with DW. The color of the prepared solutions was compared by visual inspection. To determine ε values of MSA-dye conjugates, UV-VIS-NIR spectrum assay was conducted and optical density (OD) was measured by Varioskan Flash screening mode at 350-850 nm.

Binding efficiencies between MSA and various dyes were measured by thin-layer chromatography at 10, 30 min, 1, 2, 6, and 24 h after incubation. TLC plates were scanned by Fujifilm LAS 3000 and the spots were quantified by multi-gauge 3.0. HPLC was used to distinguish the size between before and after dye and MSA conjugation. Fluorescence imaging was performed at 420-780 nm excitation and 520-845 nm emission to find out the wavelength band which exhibits strong fluorescence for MSA-dye conjugates. To evaluate the ability of MSA-NBB conjugate for SLN mapping, MSA-NBB conjugate or only NBB was injected to a same male BALB/c mice and visible and fluorescence images were obtained at 10, 30 min, 1, and 2 h post-injection. For SPECT/CT imaging, MSA-NBB conjugate was labeled with ^{99m}Tc and the conjugate complex was subcutaneously injected into the left footpad of the mouse. SPECT/CT images were obtained at 10, 30 min, 1, and 2 h after injection.

Results:

All dyes that were used in visible screening showed a clear color at 0.25 mM. As dilution, some dyes were difficult to identify color of the solution and NBB, PBVF, NY, BR and EB showed most visible at low concentration at 0.004 mM. In order to compare each of MSA-dye conjugates by a quantified value, ε values were calculated by Beer-Lambert Law using OD values at peak wavelength. MSA-PBVF conjugate demonstrated the highest ε value of 141,481 $M^{-1} \cdot cm^{-1}$,

followed by MSA-EB conjugate (99259.3), MSA-ICG conjugate (87037.0) and MSA-NBB conjugate (62222.2). Size exclusion HPLC confirmed that MSA-dye conjugates was formed as a monomer. All the prepared MSA-dye conjugates was stable for 24 h and no other aggregates were found in the chromatogram. TLC results showed that binding efficiencies of all dyes were increased depending on the concentration of MSA and the reaction time. Especially, NBB had the highest binding affinity with MSA among all the tested dyes requiring the least amount of MSA (2.5 mg) and the short reaction time (10 min). Binding ratio was calculated that 0.7 of NBB was bound with 1.0 of MSA. Based on these results, NBB was selected for the *in vivo* application. Fluorescence of MSA-NBB conjugate was detected at excitation 600 nm, emission 670 nm and fluorescence of unbound dyes or MSA was not detected at the same range. In visible image, MSA-NBB conjugate accumulated more in the popliteal lymph node that NBB alone at all the investigational time. The fluorescence of MSA-NBB conjugate and NBB alone were accumulated in the popliteal LN at 10 min at 4.48±0.34 and 4.24±0.18 flux (10^8 p/s), respectively. While the fluorescence of MSA-NBB conjugate in the popliteal LN was maintained for 2 h (4.81±1.24 flux (10^8 p/s)), the fluorescence of NBB alone rapidly decreased (2.61±0.46 flux (10^8 p/s)). MSA-NBB conjugate showed about two-fold higher popliteal LN uptake as compared with NBB alone from 30 min to 2 h after footpad injection. In SPECT/CT images, ^{99m}Tc-MSA-NBB conjugate was highly accumulated in the popliteal and inguinal LN. The SUV_{mean} value of ^{99m}Tc-MSA-NBB conjugate in the popliteal and inguinal LN was 13.08±2.33 and 3.00±1.64 at 10 min and 17.83±5.85 and 4.99±3.44 at 2 h,

respectively. SPECT/CT results showed that the popliteal LN uptake of ^{99m}Tc-MSA-NBB conjugate was about 3.5-fold higher than inguinal LN uptake at all time points.

Conclusion:

In this study, ^{99m}Tc-MSA-NBB conjugate was developed as a multimodal SLN mapping agent for direct visualization, fluorescence and SPECT/CT. The ability of ^{99m}Tc-MSA-NBB conjugate for accumulation in SLN was assessed by evaluating the popliteal LN uptake which is closest to the foot pad by visual monitoring, fluorescence imaging, and SPECT/CT. The results demonstrated that ^{99m}Tc-MSA-NBB conjugate binds quickly to SLN and accumulates in SLN until 2 h after footpad injection. Based on these results, ^{99m}Tc-MSA-NBB conjugate has a great potential as an SLN mapping agent for clinical use.

Key Words: mannosylated human serum albumin; sentinel lymph node mapping; image-guided surgery; blue dye; lymphoscintigraphy; multimodal;

Student number: 2014-30667

Contents

List of Figures and Tables

List of Abbreviations

Full name	Abbreviation
Sentinel lymph node	SLN
Lymph node	LN
Mannosylated human serum albumin	MSA
Evans blue	EB
Naphthol blue black	NBB
Patent blue VF	PBVF
Reactive blue 4	RB4
Nitrazine yellow	NY
Indocyanine green	ICG
Brilliant blue R	BR
Brilliant blue G	BG

Evans blue	**EB**
Single photon emission computed tomography	**SPECT**
Computed tomography	**CT**
Human serum albumin	**HSA**
Thin-layer chromatography	**TLC**
Instant thin-layer chromatography silica gel	**ITLC-SG**
High performance liquid chromatography	**HPLC**
Dynamic light scattering	**DLS**
Standardized uptake values	**SUV**
Distilled water	**DW**
Near-infrared	**NIR**
Ethylenediaminetetraacetic acid	**EDTA**

Methanol	**MeOH**
Dichloromethane	**DCM**
Ultraviolet	**UV**
Optical density	**OD**
3-Dimensional regions of interest	**3D ROI**
Positron emission tomography	**PET**
Magnetic resonance imaging	**MRI**
4-(2-Hydroxyethyl)piperazine-1-ethanesulfonic acid	**HEPES**
2-(N-morpholino)ethanesulfonic acid	**MES**
(N-(3-dimethylaminopropyl)-N'-ethylcarbodiimide hydrochloride	**EDCI**

INTRODUCTION

Sentinel lymph node (SLN) is the first regional lymph node (LN) existing nearest to the primary tumor. The detection of SLN in breast cancer and melanoma patients is important to evaluate tumor staging or to establish therapeutic decision-making. (*1-8*).

Blue dyes (*1, 2, 9-12*) or radiotracers (*3, 13-16*) have been used for the detection of SLN; however, both methods have some limitations. Although blue dyes may visualize SLN directly during surgery and allow accurate identification of SLN without any special instrument or device (*1, 2, 9-12*), these dyes are invisible under the skin or other tissues. Moreover, blue dyes rapidly diffuse to LNs adjacent to SLN due to small size (< 2 nm), thereby posing difficulty in the detection of SLN. Radiotracers with small size (< 10 nm) such as ^{99m}Tc-mannosylated human serum albumin (MSA) (*17-24*) or ^{99m}Tc-DTPA-mannosyl-dextran (or ^{99m}Tc tilmanocept) (*25-34*) have been developed for targeting mannose receptor (CD206) on the surface of macrophage. Although ^{99m}Tc-DTPA-mannosyl-dextran had advantages of low toxicity (*27, 29*) and rapid elimination from the injection site (*27, 29*), it could diffuse into not only lymphatic system but also blood circulation (*27, 29*). Moreover, ^{99m}Tc-DTPA-mannosyl-dextran did not show significantly improved SLN uptake compared to a non-receptor targeting probe, filtered ^{99m}Tc-sulfur colloid (*27*). Radiotracers such as ^{99m}Tc-sulfur colloid (~100 nm) may effectively localize SLN (*3, 13-16*) but experienced surgeons are required to increase SLN detection rate and accuracy (*35, 36*). In addition, the amounts

entering the lymphatic system are very low and most of the ^{99m}Tc-sulfur colloid remains in the interstitial tissue of the injection site due to the large size.

Combined radiotracer and blue dye method (*8, 13, 37-45*) was used for SLN mapping to take advantage of the benefits from two methods (*37, 42*). In breast cancer patients, the detection rate increased from 73% to 92%, and false negative rate decreased from 7.6% to 4.5% with the combination method compare to blue dye method (*37, 42*). Even inexperienced surgeons could achieve low false-negative rate with the combination method (*37, 42*). However, as the migration rate of blue dye and radiotracer through the lymphatic system is inconsistent, the combination method requires separate injection of blue dye and radiotracer. Therefore, surgery procedure could be complicated because a radiotracer is injected before surgery and a blue dye is administered during surgery.

In order to simplify the procedure, radiolabeled blue dyes such as ^{99m}Tc-evans blue (EB) (*46, 47*) and ^{68}Ga-EB (*48*) have been developed. These radiolabeled blue dyes enabled SLN mapping with single administration prior to the surgery. In fact, SLN mapping using ^{99m}Tc-EB could be done within 10 min post-injection (*46, 47*). However, rapid diffusion into other LN or tissues was a serious problem in localizing SLN. Therefore, it was necessary to develop blue dye-radiotracer conjugate having the same migration properties and staying longer in SLN. Development of such a multimodal imaging agent is required to overcome the limitations of blue dye, radiotracer or the combined method.

In the present study, the goal was to develop a new multimodal SLN

mapping agent which more accurately detects SLN by complementing the disadvantage of existing methods. The most important factors in SLN mapping agent development were as follows; (1) SLN visualization without special instrument or device during surgery, (2) identification of SLN which is located deep in the skin and other tissues, (3) long accumulation of the agent in SLN without diffusion to distal LN or other tissues. First, to visualize SLN, several dyes for SLN mapping during surgery was selected by referring to a literature, which bind to albumin and MSA with high affinity and exhibit a strong dark blue color; naphthol blue black (NBB), patent blue VF (PBVF), reactive blue 4 (RB4), nitrazine yellow (NY), indocyanine green (ICG), brilliant blue R (BR), and brillian blue G (BG) (**Figure 1**) (*49*). Second, ^{99m}Tc, a radioisotope with high tissue penetration was used to identify SLN deep in the skin. Radioisotope was expected to be available for lymphoscintigraphy as well as direct visualization during surgery. Third, MSA which has been developed for targeting macrophage mannose receptor (CD206) (*17-24*) was used. MSA could be accumulated in SLN due to suitable size and receptor targeting ability. Especially, MSA is able to be labeled with ^{99m}Tc, and binds well to the dye; thus, it is suitable for use as a multimodal agent. It is known that most of the dyes have a property of binding to albumin (*50*) and clinicians have used dyes to measure the concentration of albumin in plasma (*51-57*). The hypothesis of this study is that ^{99m}Tc-MSA-dye conjugate can be produced by simple mixing, and the prepared ^{99m}Tc-MSA-dye conjugate has an ability to detect SLN via direct visualization or lymphoscintigraphy. In addition, due to the properties of MSA, it can accumulate in SLN and show temporary

retention. To confirm these hypotheses, various dyes were tested for binding efficiency to MSA, and the selected MSA-dye conjugates were investigated for its ability for SLN localization using visual investigation, fluorescence imaging, and single photon emission computed tomography (SPECT)/computed tomography (CT).

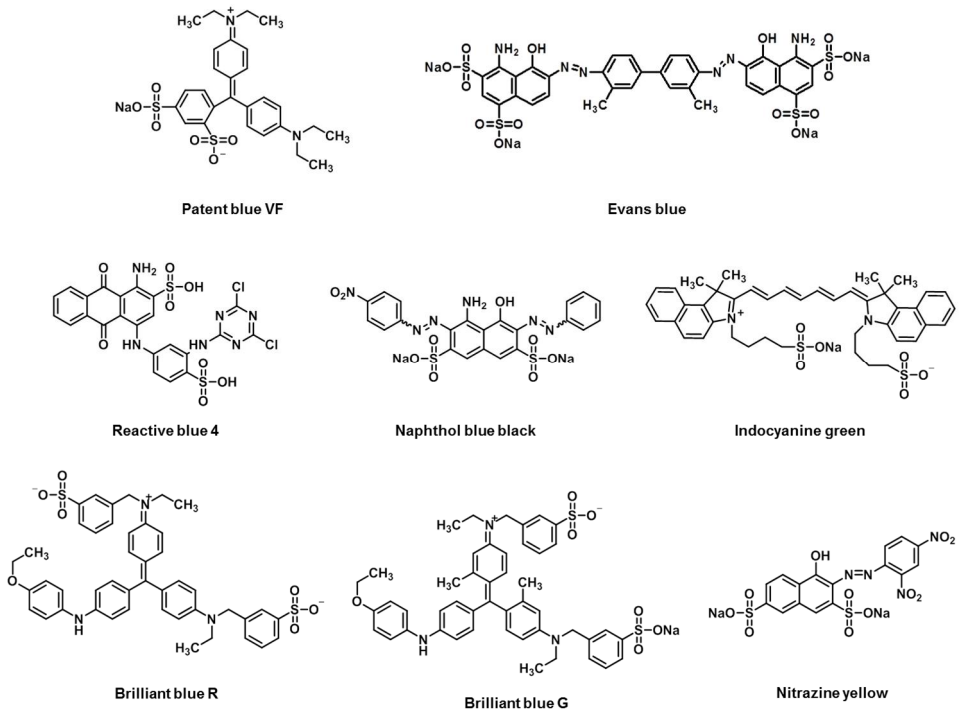

FIGURE 1.

Molecular structure of dyes. Patent blue VF (PBVF), nitrazine yellow (NY), naphthol blue black (NBB), reactive blue 4 (RB4), indocyanine green (ICG), brilliant blue R (BR), brilliant blue G (BG) and evans blue (EB).

MATERIALS AND METHODS

Human serum albumin (HSA) solution (20%) was obtained from Green Cross Corporation (Seoul, Korea). PBVF, NY, RB4, BR, BG, EB, and α-d-mannopyranosylphenyl isothiocyanate were purchased from Sigma-Aldrich (St. Louis, MO, U.S.A.) and NBB and ICG, from Tokyo chemical industry Co. (TCI, Japan). All other reagents and solvents were supplied by Sigma-Aldrich (St. Louis, MO, U.S.A.).

Sephadex G-25 column (PD-10, Pharmacia, Uppsala, Sweden) was used for the purification of MSA. Thin-layer chromatography (TLC) silica gel $60F_{264}$ (Sigma-Aldrich, St. Louis, MO, U.S.A.) was used for the determination of binding efficiencies. Instant thin-layer chromatography silica gel (ITLC-SG) plate was purchased from Agilent Technologies (Santa Clara, CA, U.S.A.).

Fujifilm LAS-3000 was purchased from Fujifilm Life Science (West Avenue, Stamford, U.S.A.). Varioskan Flash (Thermo Fisher scientific Inc., Waltham, Massachusetts, U.S.A.) was used for UV-VIS-NIR screening. Fluorescence images were obtained using IVIS Lumina II (Caliper Life Science, Hopkinton, Massachusetts, U.S.A.) and Igor Pro 4.09A (Wave Metrics Inc., Portland, Oregon, U.S.A.). ^{99m}Tc-pertechnetate was eluted from ^{99}Mo/^{99m}Tc-generator (Sam Young Unitech Co., Korea). Bio-Scan AR-2000 scanner (Bioscan, WI, U.S.A.) was used for the measurement of radiochemical purity. To determine the size of MSA-dye conjugates and ^{99m}Tc-MSA, HPLC (Gilson Inc., Wisconsin, U.S.A.), TSK gel G4000SW_{XL} column (Tosho Bioscience GMbH, Griesheim,

Germany) and a dynamic light scattering (DLS) system Zetasizer Nano ZS90 (Malvern Instruments Ltd, Worcestershire, UK) were used. SPECT/CT were obtained using NanoSPECT/CT^{Plus} (Mediso, Budapest, Hungary) and analyzed with DICOM browser in InVivoScope (IVS) program.

Animal studies were performed at the Seoul National University Hospital (Seoul, Korea), which was accredited by AAALAC International (2007, Association for Assessment and Accreditation of Laboratory Animal Care International). Male BALB/c mice (4-week-old) were purchased from OrientBio (Seoul, Korea) and housed in 5 animals per cage at 22±2℃, humidity of 40-60% and 12 h light/dark cycle. All of the animal studies were approved by Institutional Animal Care and Use Committee of the Clinical Research Institute and performed in accordance with the National Research council guidelines from the institute.

Preparation of MSA and kits for ^{99m}Tc labeling

MSA was prepared as previously described with minor modification (*19*). Briefly, HSA (20 mg) and α-d-mannopyranosylphenyl isothiocyanate (5.5 mg) were added to 5 mL of 0.1 M sodium carbonate buffer (pH 9.5). The mixture was reacted at room temperature for 20 h with continuous stirring, followed by purification with PD-10 size-exclusion column using distilled water (DW). The purified MSA was freeze-dried and stored at −20℃ until analysis.

MSA kit was prepared for ^{99m}Tc labeling according to the previously described procedure with minor modification (*17*). Briefly, HSA (10.7 mg) was dissolved in 1 mL of 0.1 M sodium carbonate buffer (pH 9.5) and treated with α-d-mannopyranosylphenyl isothiocyanate (1 mg) at room temperature for 20 h with continuous stirring. For reduction of MSA, 40 μL of 0.3 M ethylenediaminetetraacetic acid (EDTA, pH 8.0), 40 μL of 1 M sodium bicarbonate, and 50 μL of 1.5 M β-mercaptoethanol were added. The reaction mixture was incubated at 37°C for 1 h and purified with PD-10 column using phosphate buffer (pH 6.0). The solution was aliquoted into vials containing 1 mg MSA, 0.25 mg sodium medronate, 80 μg sodium ρ-aminobenzoate, and 13.6 μg stannous fluoride per vial. The vials were freeze-dried and store at −20°C for further studies.

In vitro visibility test of dyes

Visible monitoring was conducted to investigate dyes that display the dark color. Each 1 mL of 1 mM dye solution in DW was serially diluted with DW from 0.25 to 0.0001 mM. The prepared solutions were monitored by visual inspection.

Absorption spectra and molar absorption coefficient (ε) of MSA-dye conjugates

UV-VIS-NIR spectrum assay was conducted to determine ε values. Each 25 μL of 1 mM dye solution in DW was added to 5 mg MSA in 50 μL of DW. The mixture was incubated at 37°C for 24 h with continuous stirring. Optical density (OD) was measured by Varioskan Flash screening mode at 350-850 nm. Values of ε were calculated according to Beer-Lambert Law. Light path was 0.54 cm and concentration of various dyes was 5 μM.

$$\varepsilon = A/L/C$$

A = optical density

L = light path-length of solution (cm)

C = concentration of solution (M)

In vitro measurements for the binding efficiencies of dyes with MSA

Binding efficiencies of various dyes to MSA were tested by adding 25 μL of 1 mM dye solution in DW into 0.625, 1.25, 2.5, 5, 10, and 20 mg MSA dissolved in 50 μL of DW. The mixture was incubated at 37°C with continuous

stirring and 0.3 μL of each mixture was spotted on TLC plate at 10 min, 30 min, 1 h, 2 h, 6 h, and 24 h after incubation. Vacuum chamber was used for drying TLC plate over 40 min before TLC development. Mobile phase TLC conditions were described in **Table 1**. Methanol (MeOH) and dichloromethane (DCM) was used as TLC eluents at 3:7 ratio for PBVF, NBB, ICG, and BR and 1:4, 1:3, and 8:5 ratio for BG, NY, and RB4, respectively. MSA-bound dyes remained at the origin and free dyes moved to the solvent front. TLC plates were scanned by Fujifilm LAS 3000 and quantified by multi-gauge 3.0. Binding efficiencies were calculated based on the TLC results.

TABLE 1.

Various conditions of mobile phase for TLC.

Dye	MeOH:MC	R_f
Patent blue VF	3:7	0.4
Naphthol blue black	3:7	0.25
Nitrazine Yellow	2.5:7.5	0.35
Reactive blue 4	8:5	0.9
Indocyanine green	3:7	0.35
Brilliant blue G	2:8	0.3
Brilliant blue R	3:7	0.7
Evans blue	5:5	0.9

Size exclusion HPLC before and after MSA and dye conjugation

Size exlclusion HPLC was used to confirm the size before and after MSA and dye conjugation. TSKgel G400SW_{XL} size exclusion column (7.8 x 300 nm) was used and the HPLC condition was isocratic 0.1 M sodium phosphate buffer (pH 6.7) for 20 min with a flow rate of 1 mL/min. Protein standards were used as the size standards: aggregated protein, thyroglobulin (MW 670,000), γ-globulin (MW 158,000), ovalbumin (MW 44,000), myoglobin (MW 17,000), vitamin B12 (MW 1,350). Each 25 μL of dyes (0.3 mM) was incubated with 5 mg MSA at 37℃ with continuous stirring. Each 5 μL of MSA-dye conjugates was injected into HPLC after 1 h and 24 h reaction. To detect MSA and dye, dual UV detection mode was used for MSA at 280nm, NBB at 620 nm, PBVF at 640 nm, RB4 at 600 nm, NY at 560 nm, and ICG at 700 nm.

Electrophoresis for the binding mechanism study of MSA and dyes

Electrophoresis was performed to understand the binding mechanism between MSA and dye. 10 mM dyes were prepared by dissolving in water and each 50 μL of the prepared dye solution was added into 5 mg of HSA in 25 μL of DW. The mixture was incubated at 37°C for 24 h with continuous stirring. 10 μL of the

mixture (HSA/dye) was added into 190 µL of 1 M EDCI. After then, 15 µL of the mixture was added into5 µL of loading buffer and 2 µL of the final sample was loaded to NuPAGE Noves Bis-Tris Gel. 5 µL of protein standard was also loaded to the gel to distinguish the sample's size. Running time was 25 min and voltage was 200 V (start 110-125 mA/gel, end 70-80 mA/gel).

The coomassie blue R stain solution was prepared to confirm the position of protein in the gel. 250 mg of the coomassie blue R was dissolved in 500 mL of MeOH and 50 mL acetic acid. Final volume was adjusted by adding 450 mL of DW. And the destain solution was prepared by mixing 150 mL of acetic acid and 100 mL of MeOH. Final volume was adjusted by adding 1750 mL of DW. After electrophoresis analysis, the gel was stained with the coomassie blue R solution for 10 s. The coomassie blue R solution was removed from the gel. The destain solution was then added to the gel to wash the coomassie blue R solution from the gel. The procedure was repeated for three times.

In vitro fluorescence monitoring of MSA-dye conjugates

To monitor fluorescence of MSA-dye conjugates, 25 µL of 1 mM dye solution was added into 0.625, 1.25, 2.5, 5, 10 and 20 mg MSA and incubated at 37°C for 24 h with continuous stirring. And then, 10 µL of MSA-dye conjugates which involved different concentrations of MSA were transferred to tube for fluorescence monitoring. 1 mM dye and MSA were prepared separately for the

fluorescence monitoring. The fluorescence monitoring range was excitation 420-780 nm, emission 520-845 nm (**Table 2**). Fluorescence images were obtained by IVIS Lumina II with 1 sec exposure time in a 10 cm field of view. LIVINGIMAGE version 2.12 (Xenogen) and IGOR version 1.24 (WaveMetrics) software were used for the analysis of the fluorescence images.

TABLE 2.

Wavelength ranges for *in vitro* fluorescent imaging.

Ex	Em	Ex	Em
420	520	540	670
	570		790
	620	560	620
	790		670
440	520		790
	570	580	670
	620		790
	670	600	670
	790		710
460	520		790
	570	620	670
	620		710
	670		790
	790	640	710
480	570		790
	620	660	710
	670		790
	790	680	790
500	570		845
	620	700	790
	670		845
	790	720	790
520	570		845
	620	740	790
	670		845
	790	760	845
540	620	780	845

In vivo visible and fluorescence experiments of MSA-NBB conjugate for the detection of SLN

The feasibility of ^{99m}Tc-MSA-NBB conjugate for visible and fluorescence imaging of SLN was tested using male BALB/c mice (5-week old, N = 12). Briefly, 30 μL of the prepared MSA-NBB conjugate was subcutaneously injected into the left footpad of the mice anesthetized with 2% (v/v) isoflurane at 1 L/min oxygen flow. For comparison, 30 μL of NBB solution (3.33 mM of NBB in DW) was injected into the right footpad of the same mice. After 10 min of injection, mice (N = 3) was sacrificed to obtain visible image, and then fluorescent image was obtained in the same mice. The same procedure were performed at 30 min (N = 3), 1h (N = 3), and 2 h (N = 3) after injection of MSA-NBB conjugate. Fluorescence images were obtained using IVIS Lumina II equipment (excitation/emission: 600/670 nm) with an exposure time of 1 s. The obtained fluorescence images were analyzed by LIVINGIMAGE version 2.12 (Xenogen) and IGOR version 1.24 (WaveMetrics) image analysis software.

Preparation for ^{99m}Tc-MSA-NBB conjugate

^{99m}Tc-pertechnetate (2 mL) was added to the MSA kit vial and incubated at room temperature for 30 min. Radiochemical purities were checked by ITLC-SG/Umezawa (ethanol:10% ammonium acetate = 1:1). ^{99m}Tc-MSA remained at the

origin and unlabeled ^{99m}Tc moved to the solvent front. Radioactivity on ITLC-SG plate was scanned and quantified using Bio-Scan AR-2000 scanner. MSA (25 mg) in 50 μL of DW was added to 25 μL of 10 mM NBB solution. The mixture was incubated at 37°C for 2 h with continuous stirring, followed by the addition of 30 μL MSA-NBB conjugate to 5 μL of ^{99m}Tc-MSA (25.6 MBq).

HPLC and DLS were used to confirm the size of MSA after reduction and ^{99m}Tc labeling. Bio-Sil SEC 250 size exclusion column (7.8 x 300 nm) was used for HPLC and the conditions were same as previously described. RI detector was used for ^{99m}Tc. HSA, MSA, MSA kit and ^{99m}Tc-MSA were diluted with DW, and filtered using a 0.2 μL pore size syringe filter before injection. The prepared sample (1 mL) was transferred into a cuvette and analyzed for tree times using Nano-ZS90 (Malvern, 633 nm lasers).

Analysis of SPECT/CT

The ability of ^{99m}Tc-MSA-NBB conjugate for SLN mapping was tested using male BALB/c mice (5-week old, N = 3). Briefly, 30 μL of the prepared MSA-NBB conjugate was mixed with 10 μL of ^{99m}Tc-MSA. ^{99m}Tc-MSA-NBB conjugate was subcutaneously injected into the left footpad of the mice anesthetized with 2% (v/v) isoflurane at 1 L/min oxygen flow. SPECT/CT was obtained at 10 min, 30 min, 1 h, and 2 h after injection using NanoSPECT/CT^{Plus}

and the acquisition time was 20 min. The obtained SPECT/CT was analyzed with DICOM browser in InVivoScope (IVS) program. In order to calculate Standard Uptake Values (SUV_{mean}), 3-dimensional regions of interest (3D ROI) were drawn on popliteal and inguinal LNs. SUVs were calculated by SUV calculator of the software using 3D ROI volume, 3D ROI radioactivity, mouse body weight, and injected dose.

$$SUV = AW/V/D$$

A = 3D ROI radioactivity (MBq)

W = mouse body weight (g)

V = 3D ROI volume (mL)

D = injected dose (MBq)

Stability test of ^{99m}Tc-MSA-NBB conjugate in *in vivo*

To confirm the stability of ^{99m}Tc-MSA-NBB conjugate in popliteal LN, the skin of the left leg of the mouse was removed after SPECT/CT. Visible images were obtained from the exposed popliteal LN, and popliteal LN was surgically removed according to the blue color as a guide. After then, the removed LN was moved on the opposite site of injection site and take SPECT/CT. SPECT/CT were obtained using NanoSPECT/CT^{Plus} and the acquisition time was 20 min.

Fluorescence images of removed LN were also obtained after SPECT/CT using IVIS Lumina II equipment (excitation/emission: 600/670 nm) with an exposure time of 1 s.

RESULTS

In vitro visibility test of dyes

In vitro visibility test was performed using Dyes (**Figure 2**). Dyes were serially diluted to compare the color of dye solutions at different concentration. NBB, EB and NY showed the strongest color at high concentration (0.25 mM). However, PBVF was the most visible at low concentration (0.001-0.004 mM) and BR, NBB, EB, and NY were also quite visible at low concentration (0.004 mM).

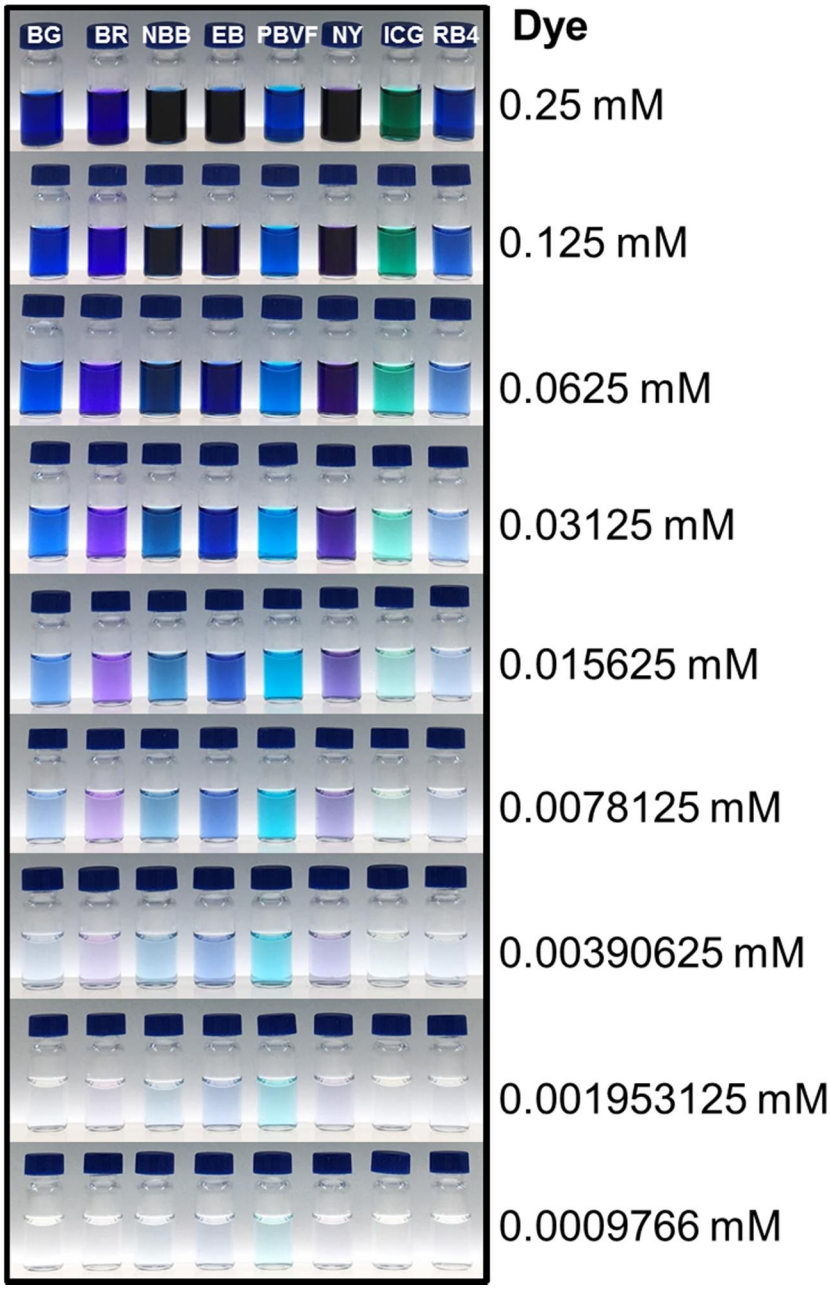

FIGURE 2.

In vitro visibility tests of dyes. Dyes were serially diluted from 0.25 to 0.001 mM.

Absorption spectra and molar absorption coefficient (ε) of MSA-dye conjugates

UV-VIS-NIR spectra of MSA-dye conjugates were obtained from 350 to 850 nm wavelengths. MSA itself showed no peak in the scanned range, while MSA-PBVF conjugate displayed a peak at 640 nm (**Figure 3**). MSA-NBB conjugate showed a peak at 620 nm with an OD value of 0.168. Values of ε were calculated with Beer-Lambert law using OD values at peak wavelength, dye concentration (5 μM), and cell length (0.54 cm) (**Table 3**). MSA-PBVF conjugate demonstrated the highest ε value of 141,481 $M^{-1} \cdot cm^{-1}$, while ε value of MSA-NBB conjugate was 62,222 $M^{-1} \cdot cm^{-1}$. It was also found that there was a wavelength difference between dye and MSA-dye conjugates (**Figure 4**). The peak wavelengths of RB4 (600 nm) and NY (460 nm) showed a UV-VIS-NIR spectral shift with RB4 of 640 nm and NY of 560 nm after MSA conjugation. Other dyes also showed a UV-VIS-NIR spectral shift: MSA-ICG conjugate at 790 mm, MSA-BR conjugate at 590 mm, MSA-BG conjugate at 620 mm and MSA-EB conjugate at 620mm. However, the peak wavelengths of NBB (620 nm) and PBVF (640 nm) were not changed before and after MSA conjugation in UV-VIS-NIR spectra.

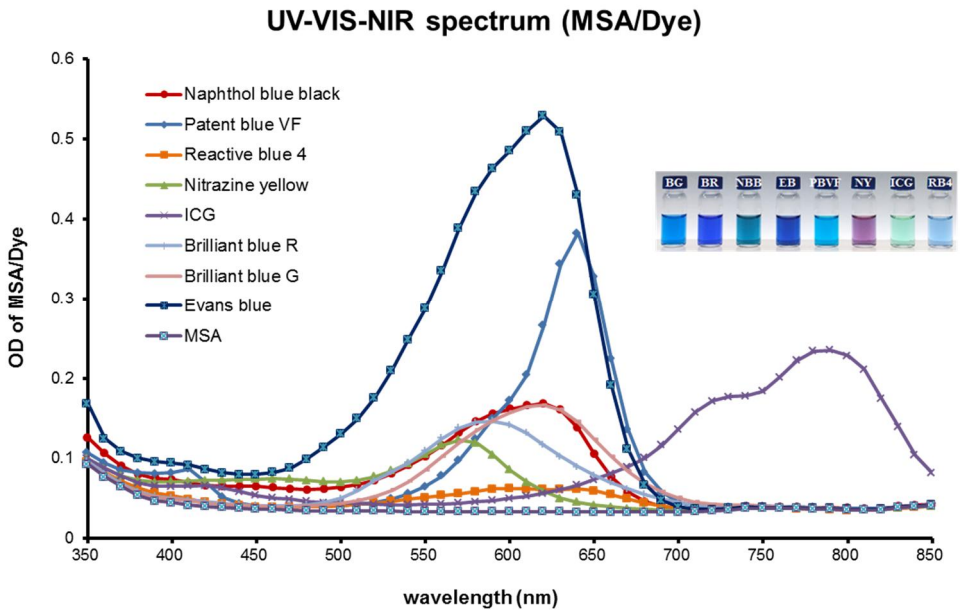

FIGURE 3.

Absorption spectra of MSA-dye conjugates. Spectra of MSA-dye conjugates scanned from 350 to 850 nm wavelengths.

TABLE 3.

Calculation of molar absorption coefficient (ε) using OD value of MSA-dye conjugates. OD values were measured at each peak wavelength of MSA-dye conjugates.

Dye (nm)	NBB	PBVF	RB4	NY	ICG	BR	BG	EB
Peak (nm)	620	640	600	560	790	590	620	620
OD	0.168	0.382	0.063	0.117	0.235	0.147	0.167	0.268
ε ($M^{-1}\cdot cm^{-1}$)	62222.2	141481.0	23333.3	43333.3	87037.0	54444.4	61851.9	99259.3

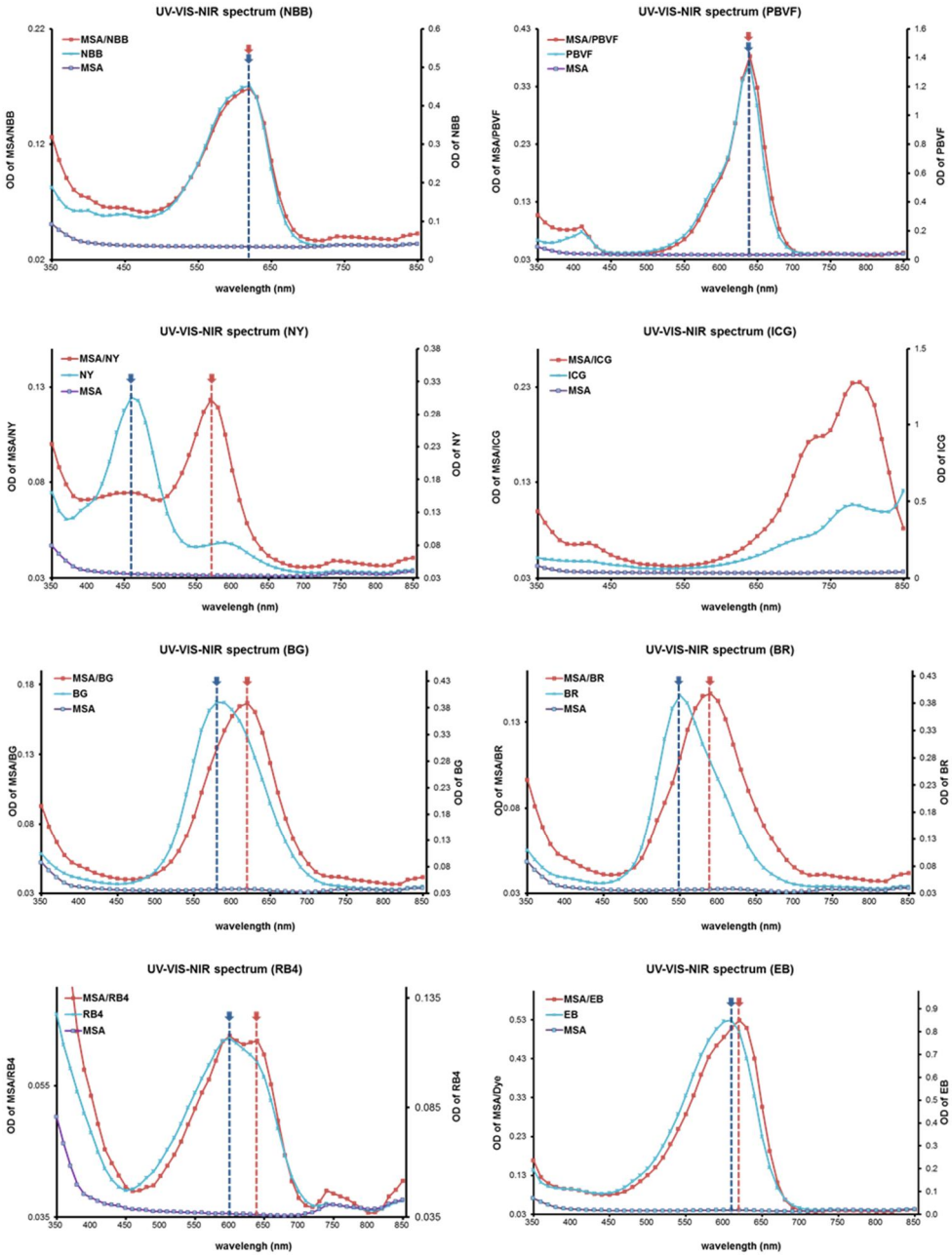

FIGURE 4.

Wavelength differences of dye and MSA-dye conjugate in UV-VIS-NIR spectra.

In vitro measurements for the binding efficiencies of dyes with MSA

Binding efficiencies of dyes with MSA were determined by TLC using different concentrations of MSA (**Table 4 or Figure 5**). ICG was excluded from the binding efficiency measurement study due to the invisibility of the color on TLC. Binding efficiencies of all of the tested dyes increased with time and concentrations of MSA. When 0.8 g/mL of MSA was used, the binding efficiency of all of the tested dyes was almost 100% within 10 min. When using 0.2 g/mL of MSA, the binding efficiency was rapidly decreased in BR and NY. NY required for the longer reaction time to achieve 100% binding, and the maximal binding efficiency of BR was 84% even in 24 h reaction. When MSA concentration was decreased to 0.1 g/mL, the binding efficiency of most dyes was decreased except PBVF, RB4 and NBB. Especially, NBB was 100% bound with MSA within 10 mins after the reaction, exhibiting the highest binding affinity among the tested dyes. RB4 also showed high binding efficiency, however, it required for 24 h for 100% binding. Based on these data, the binding ratio (mol/mol) of dyes to MSA was calculated (**Table 5**). When 25 nmol of NBB showed 100% binding efficiency with 2.5 mg MSA (35.21 nmol) at 10 min of reaction, the binding ratio was calculated to be 0.71. The binding ratio of other dyes was also calculated using the amount of dye for 100% binding with MSA: PBVF and RB4 were 0.36, BG and EB were 0.17, and NY and BR were 0.09.

TABLE 4.

Binding efficiencies of MSA and dyes (N = 3, Mean ± SD).

Dye	MSA (g/mL)	Binding percentage of MSA and dye (%)					
		10 min	30 min	1 h	2 h	6 h	24 h
PBVF	0.8	100.0±0.0	100.0±0.0	100.0±0.0	100.0±0.0	100.0±0.0	100.0±0.0
	0.4	100.0±0.0	100.0±0.0	100.0±0.0	100.0±0.0	100.0±0.0	100.0±0.0
	0.2	100.0±0.0	100.0±0.0	99.7±0.5	100.0±0.0	100.0±0.0	99.9±0.1
	0.1	61.6±0.3	86.6±0.8	88.4±0.5	90.6±0.6	90.8±0.3	91.2±0.1
	0.05	38.8±0.2	48.0±0.3	52.5±0.1	55.4±0.2	62.5±0.5	62.7±0.6
	0.025	16.6±0.3	24.3±0.4	36.3±0.1	43.0±0.6	44.2±0.1	47.4±0.2
NBB	0.8	100.0±0.0	100.0±0.0	100.0±0.0	100.0±0.0	100.0±0.0	100.0±0.0
	0.4	100.0±0.0	100.0±0.0	100.0±0.0	100.0±0.0	99.8±0.3	100.0±0.0
	0.2	100.0±0.0	100.0±0.0	100.0±0.0	100.0±0.0	100.0±0.0	100.0±0.1
	0.1	100.0±0.0	100.0±0.0	100.0±0.0	98.8±0.2	98.4±0.5	100.0±0.0
	0.05	72.2±0.8	72.7±0.4	73.1±0.4	75.1±0.5	80.0±0.6	98.3±0.4
	0.025	48.4±0.5	50.6±0.4	51.3±0.0	51.8±0.5	61.1±0.5	63.8±0.2
NY	0.8	100.0±0.0	100.0±0.0	99.9±0.2	99.6±0.4	100.0±0.0	99.9±0.1
	0.4	90.4±0.5	91.6±0.5	92.8±0.4	93.6±0.4	99.6±0.6	99.9±0.2
	0.2	70.4±0.3	73.7±0.3	77.1±0.3	82.0±0.2	96.3±0.6	99.7±0.3
	0.1	50.3±0.6	50.9±0.2	63.9±0.4	73.9±0.7	87.9±0.5	99.5±0.5
	0.05	36.1±0.6	37.2±0.5	44.4±0.3	56.7±0.2	63.4±0.4	92.7±0.3
	0.025	21.5±0.5	22.1±0.3	27.6±0.7	30.6±0.6	36.8±0.3	66.3±0.4

Dye	MSA (g/mL)	Binding percentage of MSA and dye (%)					
		10 min	30 min	1 h	2 h	6 h	24 h
RB4	0.8	100.0±0.0	100.0±0.0	100.0±0.0	99.8±0.3	100.0±0.0	99.7±0.5
	0.4	100.0±0.0	99.9±0.2	100.0±0.0	100.0±0.0	100.0±0.0	99.9±0.1
	0.2	99.8±0.4	97.0±0.8	94.0±0.1	94.6±0.5	97.1±0.3	99.8±0.3
	0.1	92.3±0.8	87.7±0.5	84.7±0.9	85.6±0.3	88.8±0.4	100.0±0.1
	0.05	84.1±0.6	82.4±0.5	80.8±0.4	83.3±0.5	86.5±0.7	100.0±0.0
	0.025	74.6±0.3	79.0±0.3	78.8±0.5	81.1±0.3	82.4±0.4	100.0±0.0
BG	0.8	100.0±0.0	100.0±0.0	100.0±0.0	100.0±0.0	100.0±0.0	100.0±0.0
	0.4	100.0±0.0	100.0±0.0	100.0±0.0	100.0±0.0	100.0±0.0	100.0±0.0
	0.2	89.0±0.3	92.0±0.5	93.6±0.7	96.0±0.4	96.8±0.7	97.1±0.3
	0.1	61.7±0.9	68.7±0.8	75.7±0.6	77.4±0.7	83.3±0.8	86.9±0.5
	0.05	46.6±0.8	52.3±0.6	61.3±0.5	63.0±0.5	69.9±0.6	76.3±0.8
	0.025	23.2±0.6	27.2±0.8	33.6±0.7	36.8±0.7	41.4±0.4	51.7±0.5
BR	0.8	100.0±0.0	100.0±0.0	100.0±0.0	100.0±0.0	100.0±0.0	100.0±0.0
	0.4	92.2±0.5	92.4±0.8	92.3±0.9	93.7±0.5	94.1±0.6	96.2±0.6
	0.2	45.4±0.9	52.7±1.0	56.5±0.4	64.5±0.8	72.1±0.2	84.3±0.9
	0.1	35.6±0.6	45.5±0.7	49.1±0.9	57.2±0.9	63.5±0.7	74.4±0.8
	0.05	28.7±0.8	38.8±0.9	41.6±0.5	47.6±0.2	59.1±0.5	66.0±0.6
	0.025	17.2±0.8	21.2±0.9	29.2±0.7	35.1±0.6	37.9±0.4	45.6±0.9
EB	0.8	100.0±0.0	100.0±0.0	100.0±0.0	100.0±0.0	100.0±0.0	100.0±0.1
	0.4	100.0±0.0	100.0±0.0	100.0±0.0	100.0±0.0	100.0±0.0	100.0±0.1
	0.2	93.1±0.4	95.2±0.5	100.0±0.1	99.9±0.2	100.0±0.0	99.9±0.2
	0.1	67.3±0.5	70.9±0.3	86.9±0.4	90.1±0.3	95.2±0.2	98.4±0.6
	0.05	35.4±0.6	39.3±0.4	70.6±0.4	73.1±0.3	77.2±0.7	82.3±0.8
	0.025	16.3±0.5	22.8±0.6	42.6±0.5	50.3±0.7	60.0±0.7	67.9±0.8

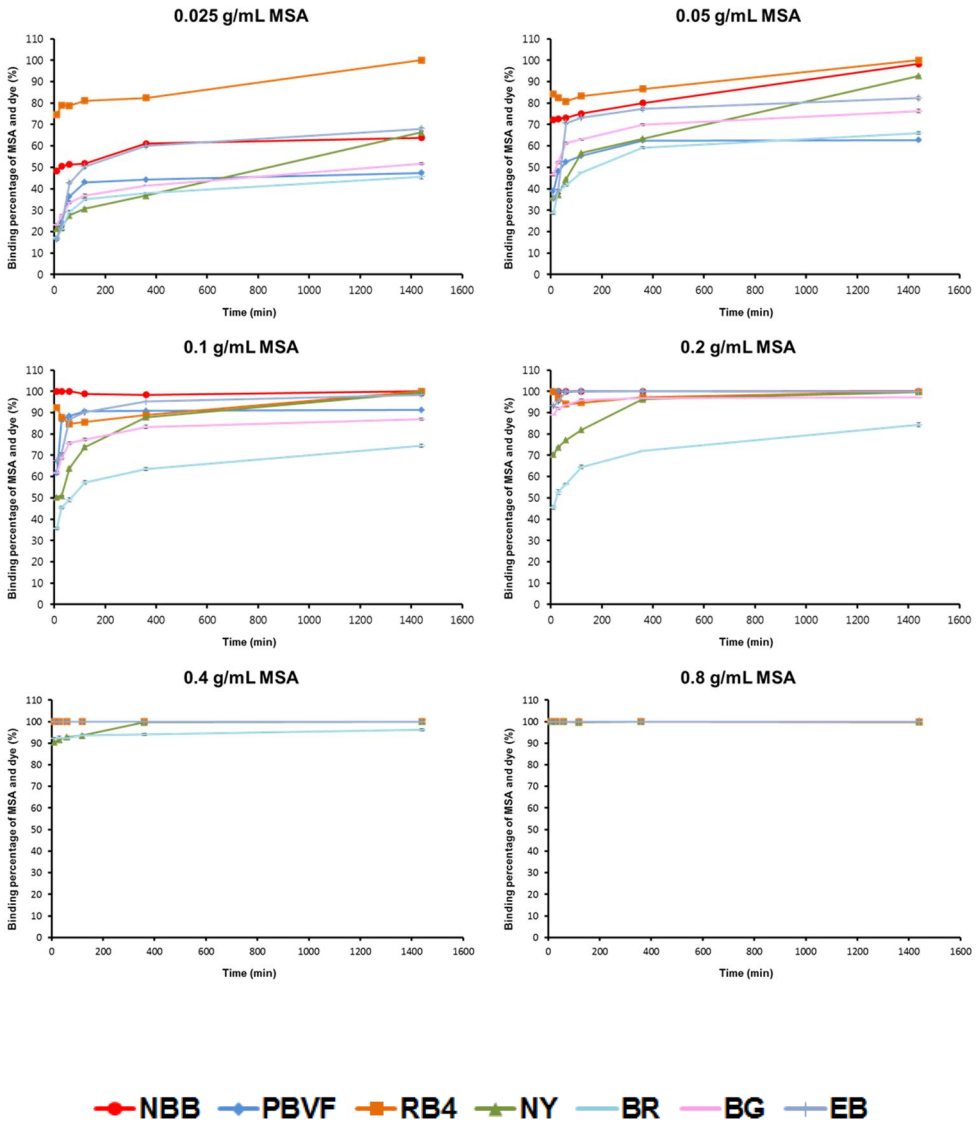

FIGURE 5.

Binding efficiencies of MSA and dyes (N = 3, Mean ± SD).

TABLE 5.

Dye/MSA ratio (mol/mol) calculated by TLC experiments (MSA: 71021).

Dye (1 mM)	MW	Purity (%)	Dye/MSA (mol/mol)
Patent blue VF	566.66	50	0.36
Naphthol blue black	616.49	>97	0.71
Nitrazine Yellow	542.36	~85	0.09
Reactive blue 4	637.43	35	0.36
Indocyanine green	774.96	-	-
Brilliant blue G	854.02	90	0.17
Brilliant blue R	825.97	-	0.09
Evans blue	960.81	75	0.17

Size exclusion HPLC before and after MSA and dye conjugation

Size exclusion HPLC was performed for monitoring of the size change before and after dye and MSA conjugation (**Figure 6**). Retention times (RT) of protein standards were 5.0-7.0 min for aggregated protein, 8.91 min for thyroglobulin (MW 670,000), 10.72 min for γ-globulin (MW 158,000), 11.3 min for ovalbumin (MW 44,000), 12.02 min for myoglobin (MW 17,000), and 12.86 min for vitamin B12 (MW 1,350). UV peak of MSA was shown at 10.92 min at 280 nm indicating that MW of MSA was between 44,000 and 158,000. On the other hand, UV peak of dye was not shown in the HPLC chromatogram from 0 to 20 min at 280 nm. Not shown in the data, UV peak of dye was detected at 40 min indicating that MW of dye was less than 1,350. RT of MSA-NBB conjugate was 10.95 min and 11.30 min after 1 h for the reaction and was not changed at all after 24 h. Other MSA-dye conjugates showed a similar pattern. Furthermore, no aggregated form was found for the investigational time.

(A) Protein standard

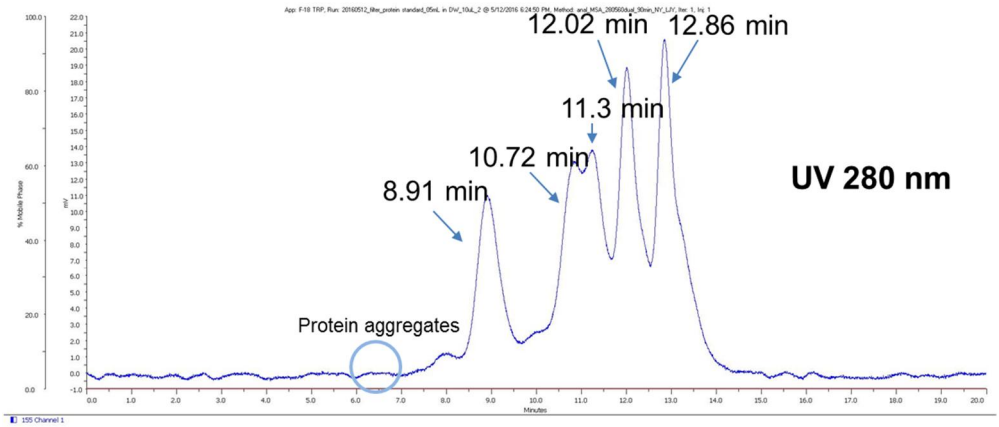

Peak Number	component	Molecular weight	Retention time (min)
1	Protein aggregates		6-7
2	Thyroglobulin	670,000	8.91
3	γ-globulin	158,000	10.72
4	ovalbumin	44,000	11.3
5	myoglobin	17,000	12.02
6	Vitamin B_{12}	1,350	12.86

(B) MSA-NBB conjugate

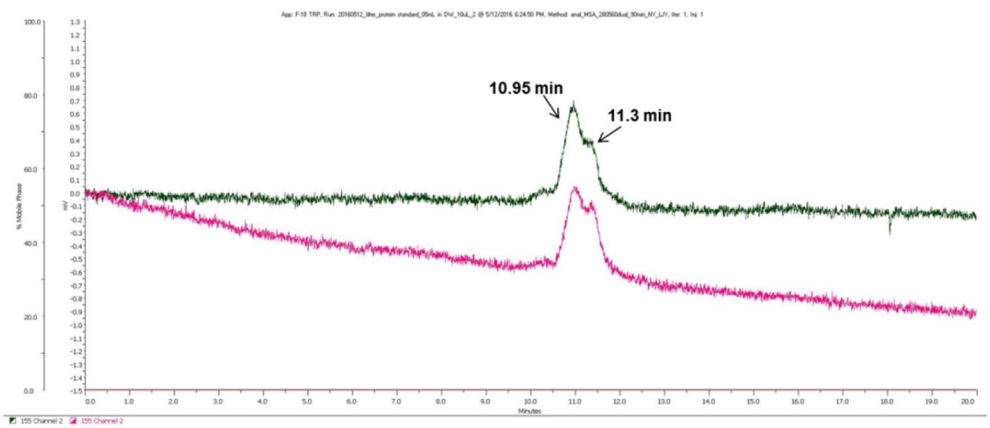

(C) MSA-PBVF conjugate

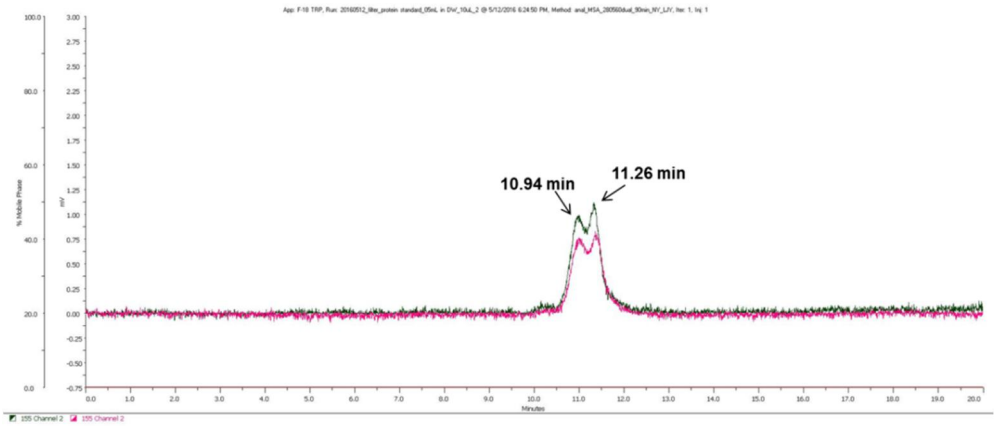

(D) MSA-RB4 conjugate

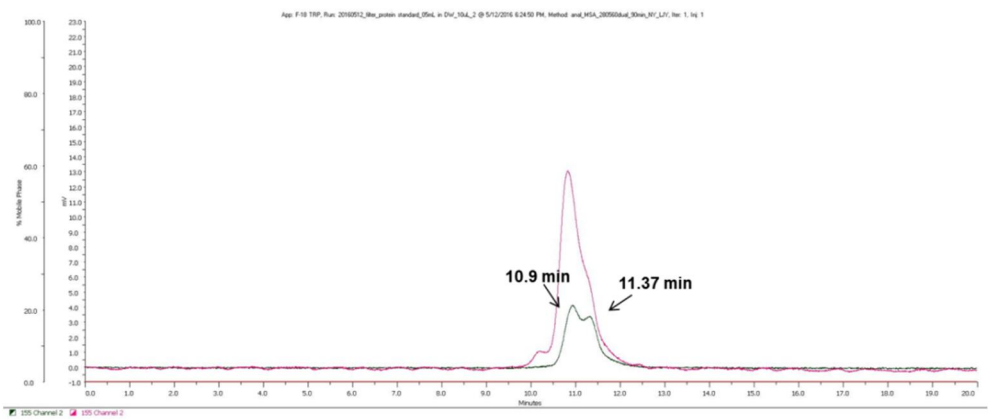

(E) MSA-NY conjugate

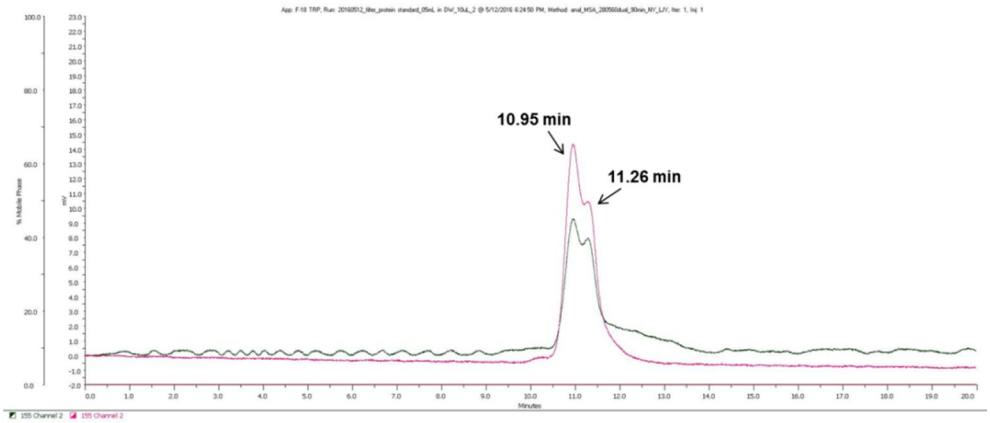

(F) MSA-ICG conjugate

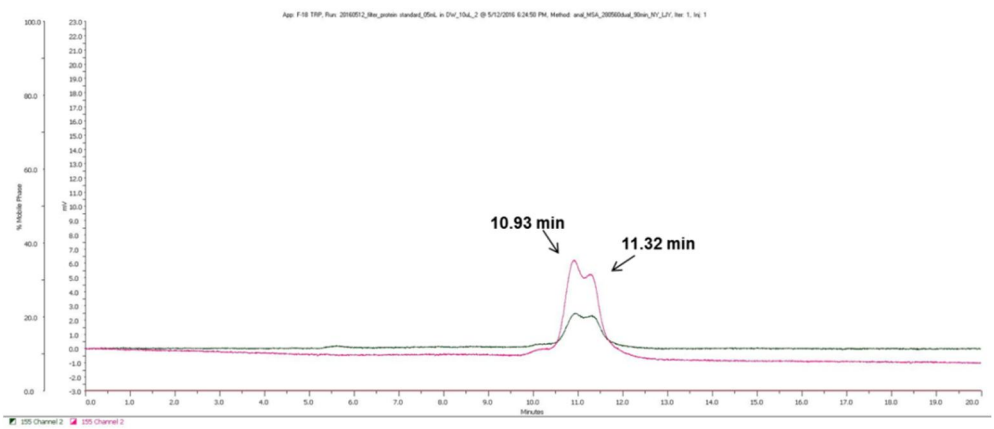

FIGURE 6.

Size exclusion HPLC chromatograms of protein standards (A) and MSA-dye conjugates (B-F). The chromatograms were obtained with UV (280 mm) at 1 or 24 h after MSA-dye conjugation using TSK gel G4000SW$_{XL}$ column (7.8 x 300 mm); 0.1 M sodium phosphate buffer (pH 6.7) for 20 min with a flow rate of 1 mL/min (Green: 1 h after MSA-dye conjugation, Red: 24 h after MSA-dye conjugation).

Electrophoresis for the binding mechanism study of MSA and dyes

The results of electrophoresis using MSA-dye conjugates were shown in **Figure 7**. Dyes were easily detected by the color, and MSA was identified after coomassie blue R staining. As soon as electricity was applied, dyes rapidly migrated to the bottom of the gel indicating low molecular weights and the positions of dyes were clearly distinguished from the position of 71,000 Daltons protein standard. But, NY showed a different result. Unlike other dyes, a little amount of NY was found at the upper of the gel which was similar level of 71,000 Daltons protein standard. As expected, MSA was found at the same level of 71,000 Daltons protein standard after staining.

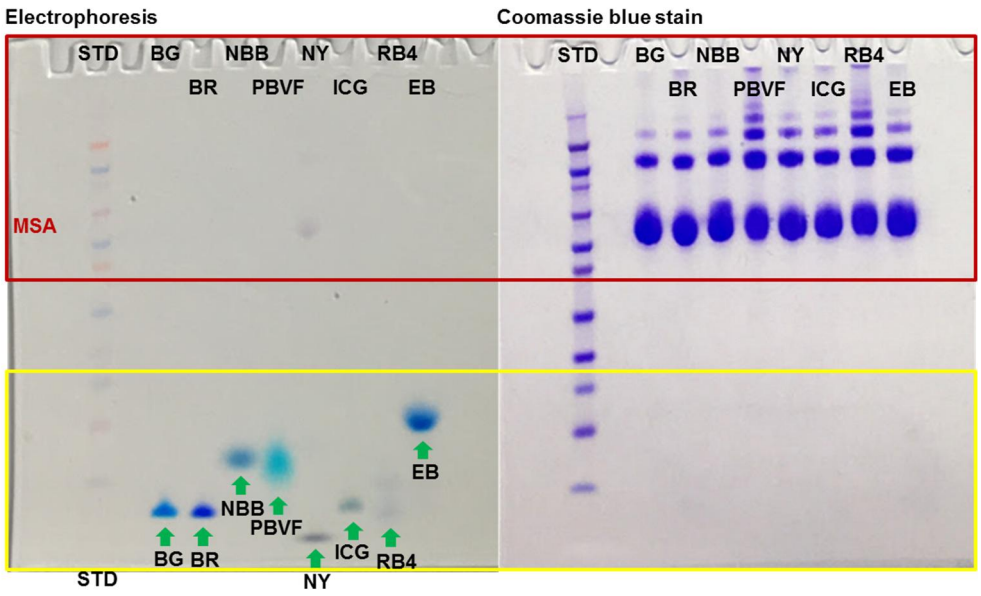

FIGURE 7.

Electrophoresis results of MSA-dye conjugates for the binding mechanism study.

In vitro fluorescence monitoring of MSA-dye conjugates

Fluorescence monitoring study was performed to find out fluorescence wavelength in which MSA-dye conjugates showed fluorescence and unbound dyes showed no fluorescence (**Figure 8**). Fluorescence wavelengths of MSA-dye conjugates were like this: MSA-BR conjugate at Ex 620 nm, Em 710 nm, MSA-BG conjugate at Ex 640 nm, Em 710 nm, MSA-NBB conjugate at Ex 600 nm, Em 670 nm, MSA-ICG conjugate at Ex 560 nm, Em 620 nm, MSA-RB4 conjugate at Ex 640 nm, Em 710 nm, MSA-PBVF conjugate at Ex 660 nm, Em 710 nm, MSA-EB conjugate at Ex 680 nm, Em 790 nm. Fluorescence of unbound dyes did not show fluorescence signal at the same wavelength. The intensity of fluorescence signal was increased with the amount of MSA and saturated at 5-10 mg of MSA.

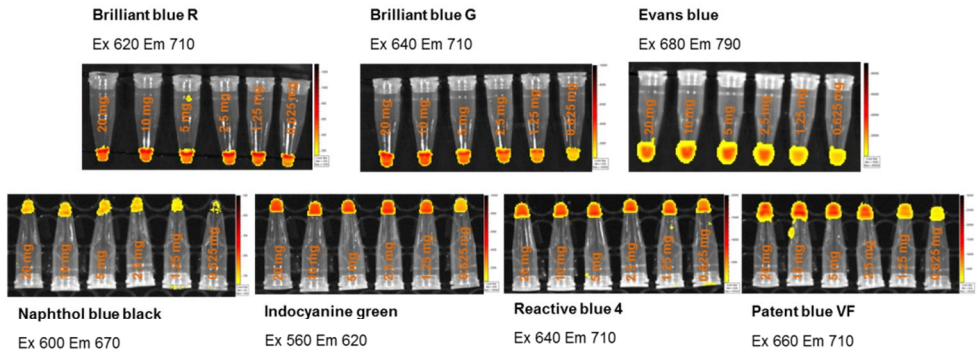

MSA	ROI (unit of counts)							
	Brilliant blue R	Brilliant blue G	Evans blue	Naphthol blue black	Indocyanine green	Reactive blue 4	Patent blue black VF	Nitrazine yellow
20 mg	51421	409470	2528300	13012	332400	600110	1171700	No signal
10 mg	55163	387730	2762800	14136	338870	607270	1244300	
5 mg	53603	352330	2830900	13340	321190	635740	1116700	
2.5 mg	54845	342200	2562200	12367	357970	554320	1020500	
1.25 mg	55731	294770	1544900	10132	325900	585710	688130	
0.625 mg	44506	182420	1060400	6561.2	206150	469070	305580	

FIGURE 8.

Fluorescence monitoring of MSA (0.625-20 mg) and dye conjugates. Fluorescence of MSA-BR, -BG, -EB, -NBB, -ICG, -RB4 and -PBVF conjugates were detected in range of excitation 420-780 nm, emission 520-845 nm and MSA-NY conjugate showed no fluorescence.

In vivo visible and fluorescence experiments of MSA-NBB conjugate for the detection of SLN

In vivo Visible and fluorescence study was performed by the protocol of **Figure 9A** and visible and fluorescence images were shown in **Figure 9B**. First, the accumulation of MSA-NBB conjugate or NBB in popliteal LN were observed by the blue color of NBB. MSA-NBB conjugate was subcutaneously injected into the left footpad of mice and the accumulation was observed in popliteal LN at 10 min. In addition, the accumulation of MSA-NBB conjugate maintained at least for 2 h after injection. For control, NBB was injected in the right footpad of the same mice and the accumulation was also shown in popliteal LN at 10 min. However, the accumulation of NBB in popliteal LN was lower than MSA-NBB conjugate and decreased at 2 h by diffusion of distal LNs.

Fluorescence images were observed in the same mice and consistent with visible images. Fluorescence was detected at 10 min even in the right popliteal LN where only NBB was injected. To compare the accumulation of MSA-NBB conjugate and NBB in popliteal LN, the intensities of fluorescence were quantified. (**Figure 9C**). The fluorescence intensities in popliteal LN at 10 min were 4.48±0.34 for MSA-NBB conjugate and 4.24±0.18 $x10^8$ flux (p/s) for NBB, respectively. After 2 h post-injection, the fluorescence intensity of MSA-NBB conjugate in popliteal LN was maintained at 4.48±0.34 $x10^8$ flux (p/s), while the fluorescence intensity of NBB was significantly decreased to 2.61±0.46 $x10^8$ flux (p/s). Fluorescence images demonstrated that the accumulation of MSA-NBB conjugate

was about 1.5-fold higher in popliteal LN as compared with NBB from 30 min to 2 h after footpad injection.

(A)

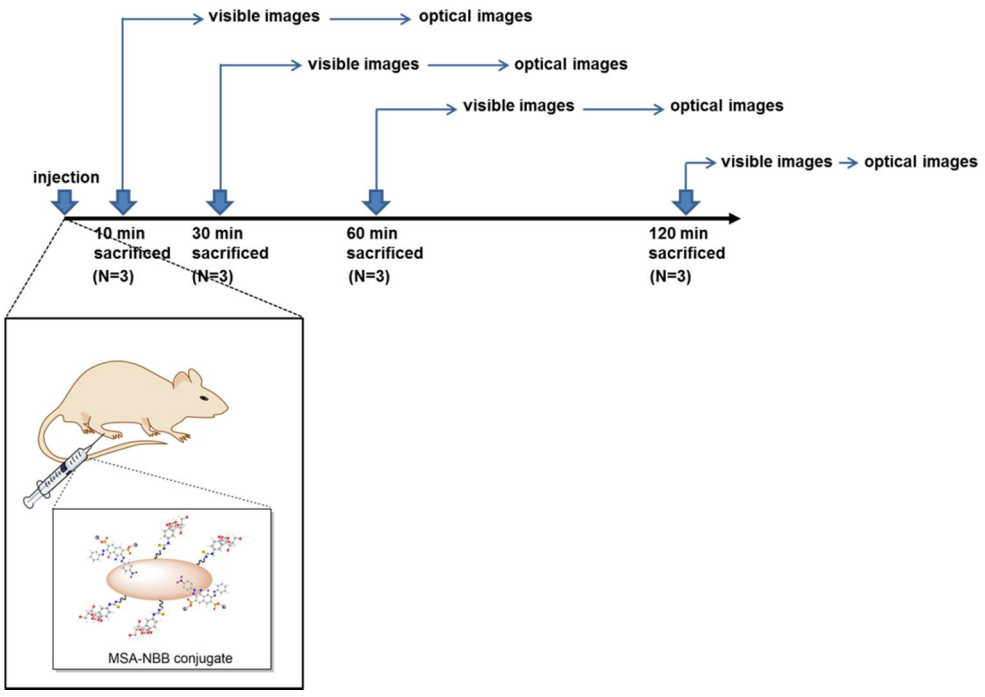
visible images
optical images
visible images
optical images
visible images
optical images
visible images
optical images
injection
10 min sacrificed (N=3)
30 min sacrificed (N=3)
60 min sacrificed (N=3)
120 min sacrificed (N=3)
MSA-NBB conjugate

(B)

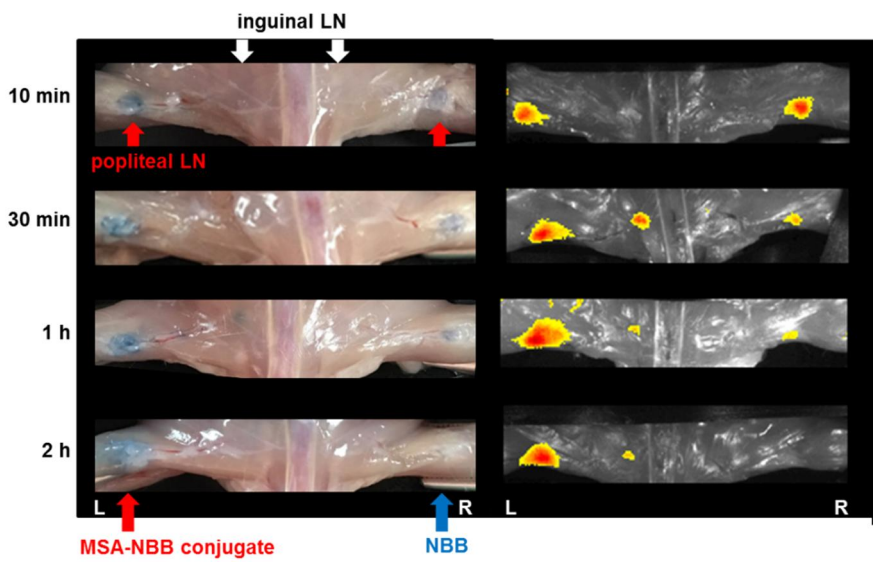
inguinal LN
10 min
popliteal LN
30 min
1 h
2 h
L
R
L
R
MSA-NBB conjugate
NBB

(C)

Total Flux x10^8 (p/s)	MSA-NBB conjugate	NBB
10 min	4.48±0.34	4.24±0.18
30 min	4.37±0.51	2.95±0.42
1 h	5.07±0.62	3.42±0.44
2 h	4.81±1.24	2.61±0.46

FIGURE 9.

In vivo visible and fluorescence experiments of MSA-NBB conjugate for SLN localization. Protocol of the experiments was shown in the scheme (A). *In vivo* visible and fluorescence images of MSA-NBB conjugate or NBB was obtained by the subcutaneous injection into footpad of mice (B). LNs were observed at 10 min, 30 min, 1 h, and 2 h after injection (N = 12, Mean ± SD) and the uptakes of fluorescence intensity were quantified respectively (C).

Preparation for ^{99m}Tc-MSA-NBB conjugate

^{99m}Tc-MSA was prepared with over 99% of radiochemical purity (**Figure 10**). Particle size distribution of HAS, MSA, MSA kit (reduced MSA) and ^{99m}Tc-MSA measured by DLS (**Figure 11**). Particle size of HSA was 5.58 nm which increased to 6.34 nm after conjugation with mannoses. The particle size of MSA increased to 9.32 nm after labeling with ^{99m}Tc due to the reduction of disulfide bonds. DLS analysis of NBB conjugated ^{99m}Tc-MSA was not possible because of the interference of blue color and fluorescence.

Size exclusion HPLC was performed to measure the size of ^{99m}Tc-MSA after radiolabeling (**Figure 12**). The retention time of ^{99m}Tc-MSA was 7.34 min at UV (280 nm) and RI, and aggregated form was also detected at 6.6 min in the chromatogram.

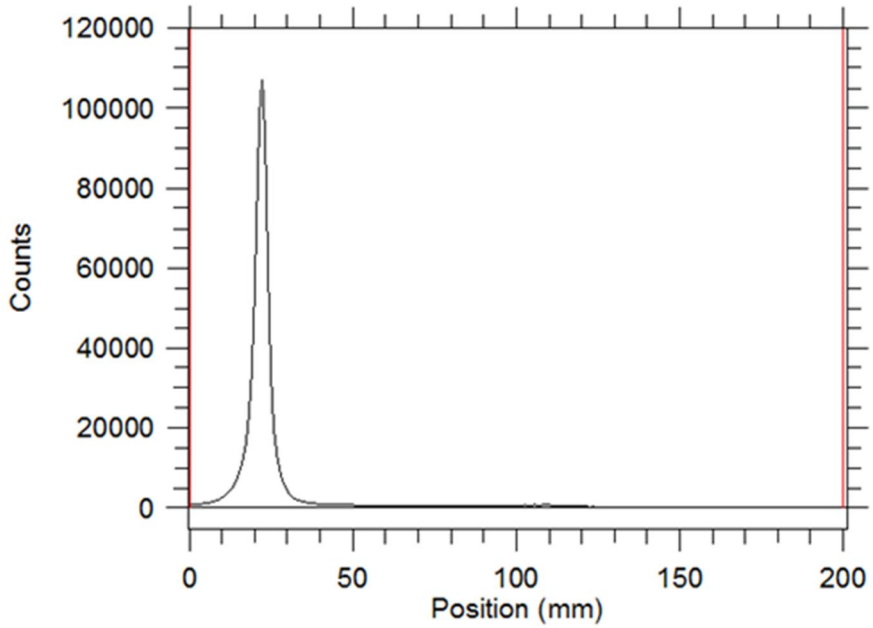

FIGURE 10.

Radiochemical purity of ^{99m}Tc-MSA determined by radio-TLC (ITLC). ^{99m}Tc-MSA remained at the origin and unlabeled ^{99m}Tc moved to the solvent front on ITLC-SG eluted by Umezawa (ethanol: 10% ammonium acetate = 1:1).

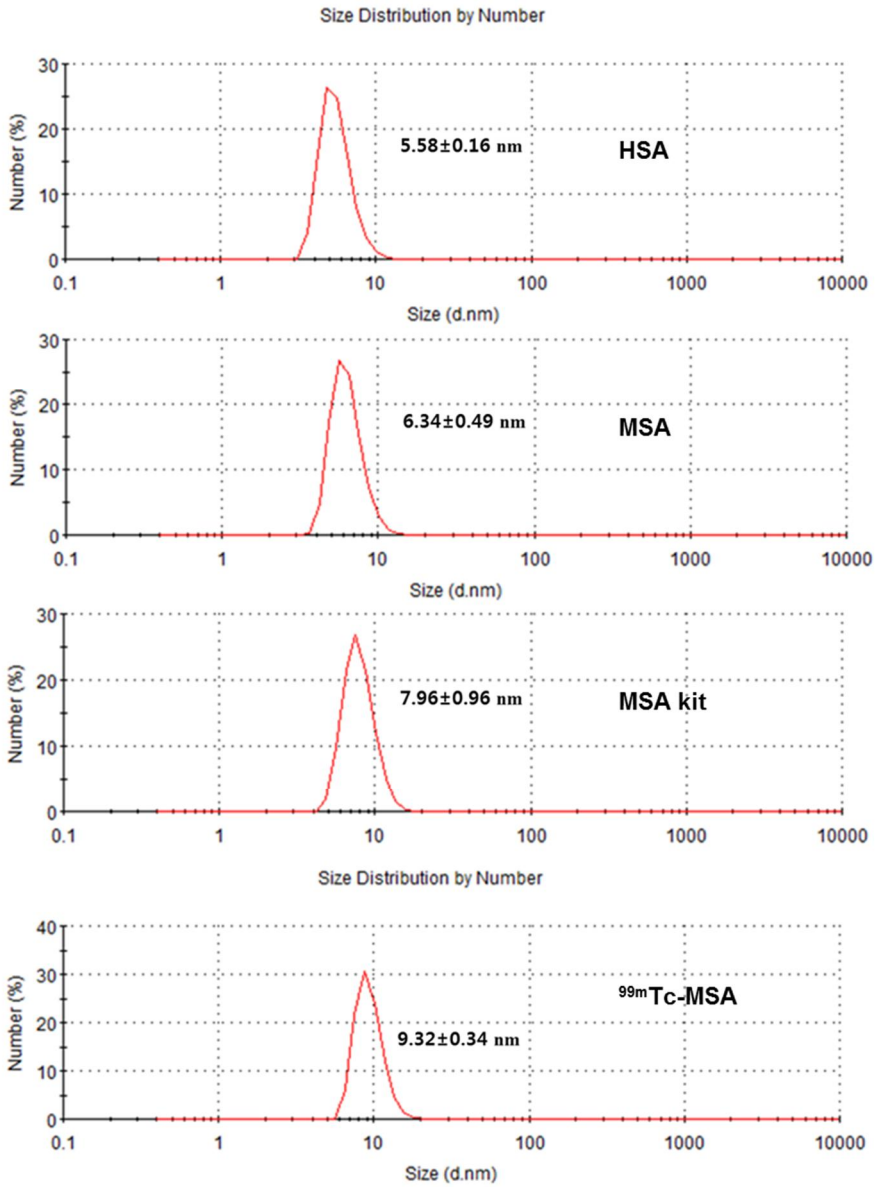

FIGURE 11.

Particle size of HSA, MSA, MSA kit (reduced MSA), and ^{99m}Tc-MSA analyzed by DLS (N = 3, Mean ± SD).

(A) Protein standard

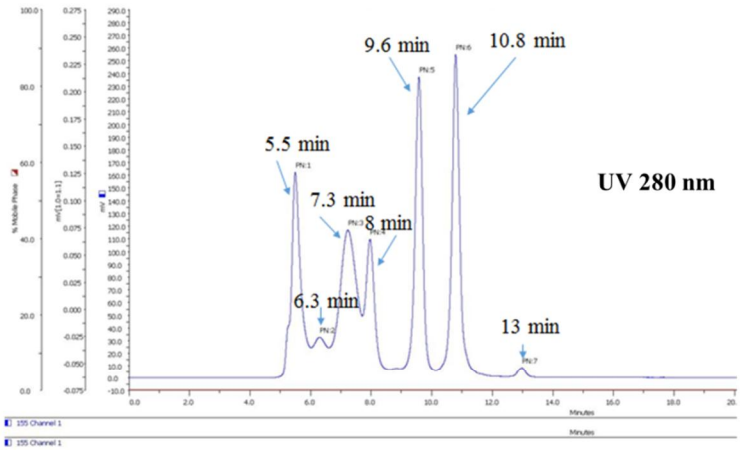

Peak Number	component	Molecular weight	Retention time (min)
1	Thyroglobulin	670,000	5.5
2	γ-globulin	158,000	7.3
3	ovalbumin	44,000	8
4	myoglobin	17,000	9.6
5	Vitamin B_{12}	1,350	10.8

(B)

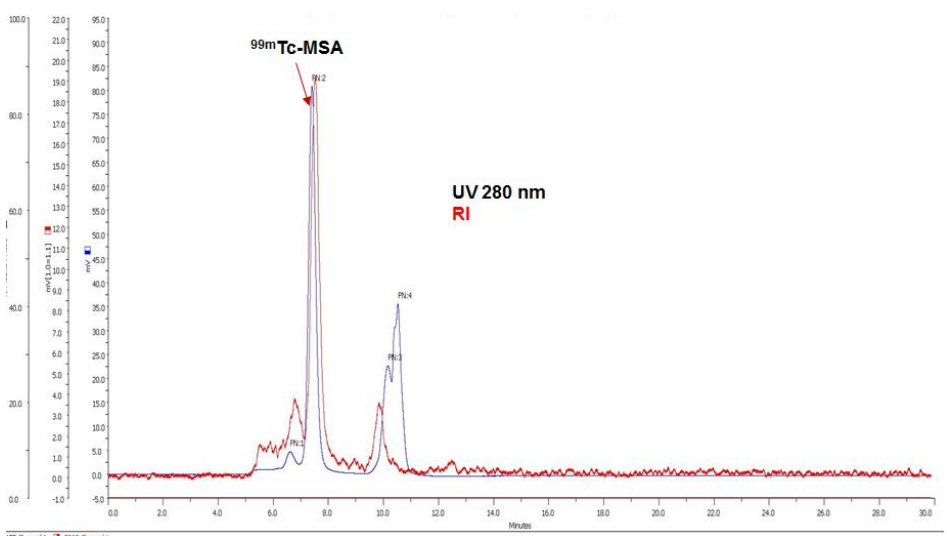

FIGURE 12.

Size exclusion HPLC chromatograms of protein standards (A) ^{99m}Tc-MSA (B). The chromatogram was obtained with UV (blue, 280 mm) and RI (red) after radiolabeling of ^{99m}Tc using TSK gel G4000SW$_{XL}$ column (7.8 x 300 mm); 0.1 M sodium phosphate buffer (pH 6.7) for 20 min with a flow rate of 1 mL/min.

Analysis of SPECT/CT

SPECT/CT was obtained at 10 min, 30 min, 1 h, and 2 h after ^{99m}Tc-MSA-NBB conjugate injection into the left footpads of mice. SPECT/CT showed the uptake of ^{99m}Tc-MSA-NBB conjugate in popliteal and inguinal LN (SUV_{mean} 13.08±2.33 and 3.0±1.64, respectively) at 10 min and the signal was maintained (SUV_{mean} 17.83±5.85 and 4.99±3.44, respectively) until 2 h after injection. SPECT/CT results revealed that popliteal LN uptake of ^{99m}Tc-MSA-NBB conjugate was about 3.5-fold higher than inguinal LN uptake at all time points.

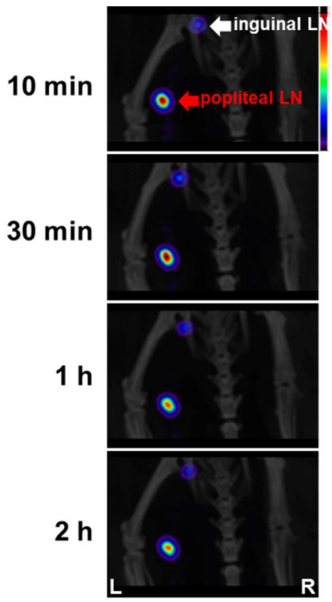

SUV_{mean}	10 min	30 min	1 h	2 h
Popliteal LN	13.08±2.33	14.68±3.63	15.97±4.63	17.83±5.85
Inguinal LN	3.00±1.64	4.21±2.97	4.75±3.59	4.99±3.44

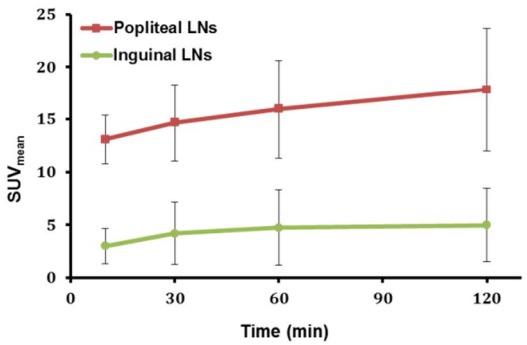

FIGURE 13.

SPECT/CT after ^{99m}Tc-MSA-NBB conjugate injection into the left footpad of a mouse (N = 3, Mean ± SD). SUVs of popliteal LN by time were quantified and plotted. Vertical bars represent SD in the graph. SUVs are almost constant until 2 h of footpad injection. Popliteal LN uptake of ^{99m}Tc-MSA-NBB conjugate was about 3.5-fold higher than inguinal LN uptake value at all time point.

Stability test of ^{99m}Tc-MSA-NBB conjugate in *in vivo*

Visible image, SPECT/CT and fluorescence images were obtained in the same mice 4 h after footpad injection to confirm the stability of ^{99m}Tc-MSA-NBB conjugate *in vivo*. Popliteal LN was found easily because of the accumulated blue color of MSA-NBB conjugate. After removing of popliteal LN according to the blue color as a guide, the radioactivity of the resected popliteal LN was observed by SPECT/CT which was placed in the opposite leg of the injection site. It was confirmed that popliteal LN was removed clearly by the blue color and SPECT/CT and popliteal LN contained ^{99m}Tc-MSA-NBB conjugate by fluorescence images.

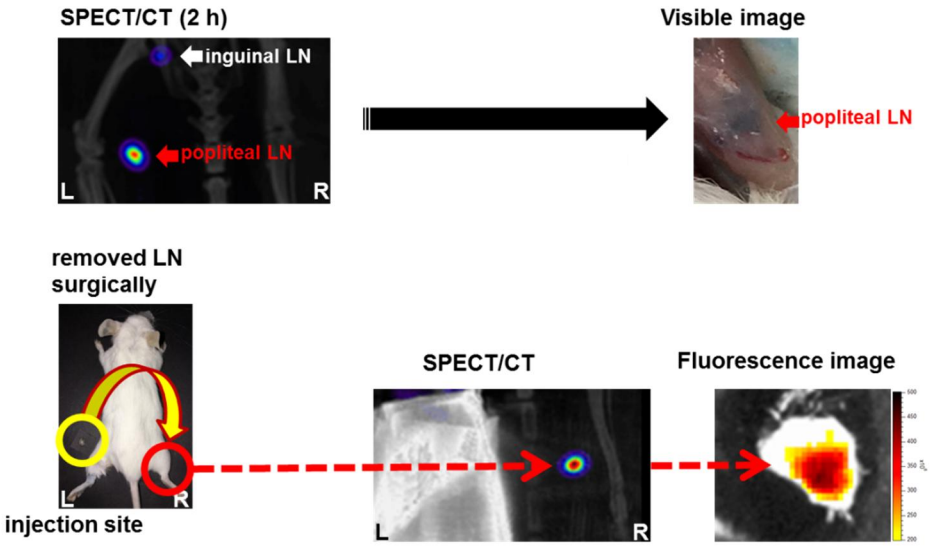

FIGURE 14.

In vivo stability tests of ^{99m}Tc-MSA-NBB conjugate.

DISCUSSION

Many studies have used blue dye to detect SLN in the surgery or radioisotopes to image SLN deep in the skin, but have experienced difficulties due to the rapid diffusion to distal LN or migration properties. Therefore, it has been expected to develop a multimodal SLN mapping agent which can visualize SLN in the surgical field without special equipment, identify SLN deep in the skin to provide information about SLN before surgery, and be stably accumulated in SLN. Such agents allow surgeons to identify the location of SLN prior to surgery and to minimize invasive surgery for cancer and metastasis by a single administration.

In the present study, MSA was used for mannose (CD206) receptors targeting which are found abundant in LNs (*58*). Previous studies showed ^{99m}Tc-MSA is rapidly accumulated in the lymphatic system, enabling SLN imaging due to the suitable molecular size of HSA (short axis, 6 nm; long axis, 8 nm) (*17, 59*). Mannose could be easily introduced by conjugation with lysine residue in HSA and it could be labeled with ^{99m}Tc after reduction of disulfide bond. Recently, efforts have been made to reduce the risk of infection by using recombinant albumin instead of albumin extracted from human blood. ^{99m}Tc-DTPA-mannosyl-dextran was developed for this purpose. However, despite approval from United States Food and Drug Administration, ^{99m}Tc-DTPA-mannosyl-dextran has not been widely used. Although this agent provides important information to localize SLN, the agent has limitations for use in the surgical field. The dissection technique depends on the operator's experience because SLN is detected only with gamma

probes during surgery. Therefore, an extra visual guide is necessary for accurate SLN localization during surgery. Blue dyes can be helpful to localize SLN in surgery. However, when blue dyes are used alone, they are not only invisible for SLN located deep inside the tissues but also difficult to be used due to the rapid diffusion into distal node. Therefore, a multimodal ^{99m}Tc-MSA-dye conjugate taking the advantages of ^{99m}Tc-MSA and blue dye was expected to be a good solution for mapping SLN accurately and efficiently.

The initial investigation was to find out suitable dye candidates for SLN visualization. According to the literature (*49*), various dyes were selected and tested for the detection of SLN. To find out dyes that produce clear color even after dilution, visual investigation was conducted using the 8 dye candidates: NBB, PBVF, NY, RB4, ICG, BG, BR and EB. All the dyes showed dark color at 0.25 mM. On the other hand, when they were diluted in 0.004 mM, BR, NBB, EB, PBVF and NY were identified. In order to quantify the value of darkness of dyes after conjugation of each dye with MSA, the molar absorption coefficient (ε) of MSA-dye conjugates was measured using the UV-VIS-NIR spectra and the Beer-Lambert Law. MSA-PBVF conjugate showed the highest ε value, and EB, ICG, NBB also showed high ε values. However, except for MSA-PBVF conjugate, there was no significant difference in color of MSA-dye conjugates. PBVF was considered the most appropriate dye, but there would be no difference in the visualization of other dyes.

Among all tested dyes, NBB showed the highest binding efficiency with

MSA within short reaction time. The binding efficiency was measured to visualize more apparent accumulation of MSA-dye conjugates in SLN. First the TLC conditions were set for each dye to distinguish dye and MSA-dye conjugates, and TLC plate was completely dried before development to reduce measurement error in quatification. Although most of dyes require at least 0.2 g/mL of MSA for 100% binding with MSA by 24 h reaction time, NBB showed 100% binding with MSA at 0.1 g/mL of MSA concentration only within 10 min. when ε value of MSA-NBB conjugate is considered, MSA-NBB conjugate may show the highest visibility in SLN. Since NBB showed not only high association with MSA, but also high visibility that is an important factor in practical applications, NBB was selected for the subsequent animal experiments.

Size of the MSA-NBB conjugate was analyzed by size exclusion HPLC and it was determined that most of MSA was conjugated with NBB as a monomer or dimer. It was needed to evaluate the size of the prepared MSA-NBB conjugate. Because aggregated MSA-dye conjugate or colloid could remain in the injection site due to the particle size (~ 100 nm), the size of MSA-NBB conjugate should be confirmed before injection to the mice. When MSA-NBB conjugate was injected into HPLC, two peaks were detected in the chromatogram. Compared to MSA chromatogram, one peak was confirmed MSA-NBB conjugate. But there was another peak right in front of it, and the peak was presumed to be that of the conjugation of dimer of MSA with NBB conjugate. Protein such as albumin has a tendency to exist not only in a single form but also in two or three forms.

NBB was non-covalently bound to MSA and the binding mechanism between MSA and dye was verified by electrophoresis analysis. It was assumed that if MSA is covalently bound to dye with σ bond, MSA and dye travel the same distance after applying electricity. On the other hand, if MSA is bound to dye with non-covalent bond such as ionic bond or hydrogen bond, MSA and dye would be easily separated. All of tested dyes were non-covalently bound to MSA but, interestingly, only NY showed a different result. The most of NY was bound to MSA with non-covalent bond, but some portion of NY seemed to be conjugated with MSA by a covalent bond.

Visible images showed the accumulation of MSA-NBB conjugate in popliteal LN. Popliteal LN is the first LN that is observed after dye injection into the mouse footpad and would be considered as SLN (*25, 26, 29, 46, 47*). Thus, to evaluate the performance for visualization of popliteal LN, MSA-NBB conjugate or NBB alone was administered into the footpad. In this experiment, experimenters were blinded for agents to minimize experimental errors and NBB was used for comparison with MSA-NBB conjugate. Dye has been used to quantify concentration of albumin because of high binding property with albumin (*50-56*), and it has been reported that LNs contain approximately 47% of albumin when compared to serum (*60*). Considering these facts, it was presumed that NBB formed albumin-NBB conjugate when NBB was transferred into lymphatic system. Thus, albumin-NBB conjugate was thought to be a good control for evaluating the performance of MSA-NBB conjugate. As a result, MSA-NBB conjugate identified

popliteal LN within 10 min and MSA-NBB conjugate was retained for at least for 2 h (the investigational time). On the other hand, although NBB showed rapid accumulation in popliteal LN at 10 min, the accumulation of NBB in popliteal LN was decreased at 2 h by diffusion of other LNs. When the amounts of the accumulation of MSA-NBB conjugate or NBB were quantified, MSA-NBB conjugate showed about 1.5-fold higher accumulation in popliteal LN than NBB from 30 min to 2 h after injection. Furthermore, fluorescence studies revealed strong fluorescence from MSA-NBB conjugate, which accumulated in the popliteal LN from 10 min to 2 h after footpad injection. From visualization and fluorescence studies, MSA-NBB conjugate showed better performance for visualization of popliteal LN than NBB which can transform into albumin-NBB conjugate by targeting to macrophage mannose receptor (CD206) in the popliteal LN. It was evident that MSA could reduce diffusion of dye into distal node and retain its accumulation in SLN. However, since LNs are deep in the skin and are invisible, use of ^{99m}Tc with good tissue penetration is necessary.

Near-infrared (NIR) fluorescence dye can visualize LNs that are located deep in the tissues. In previous studies, ICG (*61, 62*) or MSA-ICG conjugate (*23, 63*) has been used for the detection of SLN by NIR imaging. Especially, MSA-ICG conjugate was known to prevent the diffusion of ICG and show improved uptake into SLN (*23, 63*). However, NIR imaging requires a special instrument to observe fluorescence and SLN localization can be achieved through a monitor. In contrast, blue dyes can be visualized directly with naked eyes, thereby facilitating the

dissection of SLN in a convenient and practical way.

^{99m}Tc-MSA-NBB conjugate accumulated in SLN and showed very low uptake in the distal LN. The uptake in popliteal LN was estimated to be approximately 3.5-fold higher than that in inguinal LN at all time points. It means that ^{99m}Tc-MSA-NBB conjugate did not follow the conventional migration property of blue dyes which are diffused quickly into distal node, and that it has characteristic to accumulate in popliteal LN until 2 h. SPECT/CT results also showed that ^{99m}Tc-MSA-NBB conjugate could provide information to identify the position of SLN before surgery.

^{99m}Tc-MSA-NBB conjugate was stably accumulated in popliteal LN until 2 h post-injection. By the previous fluorescence monitoring, it was known that only MSA-dye conjugate exhibited fluorescence at specific wavelength and MSA or dye itself did not. The accumulation of ^{99m}Tc-MSA-NBB conjugate was examined by the observation of popliteal LN after SPECT/CT. Blue color in popliteal LN after 2 h proposed the accumulation of MSA-NBB conjugate and the radioactivity and fluorescence from the resected popliteal LN indicated the existence of ^{99m}Tc and MSA-NBB conjugate. Otherwise, ^{99m}Tc and MSA-NBB conjugate may show the same migration properties with NBB by diffusing to distal LNs. Therefore, ^{99m}Tc-MSA-NBB conjugate can be used as the multimodal imaging agent.

Currently, as the need for image-guided surgery is increasing, the development of multimodal SLN mapping agents is necessary to provide advanced options for future progress in surgery. ^{99m}Tc-MSA-NBB conjugate developed in

this study has to be supplemented by further studies. The limitations of this study are as follows; (1) limitation in serial animal experiment, (2) comparison with other SLN mapping agents, (3) new approach method using other dyes. First, it would have reduced experimental errors to obtain serial images using same mice when visual assessment and fluorescence imaging were performed after injection. Second, ^{99m}Tc-MSA-NBB conjugate should have been compared with other SLN mapping agents, which are widely used in practice, to increase the competitiveness. Third, in order to increase the sensitivity of visible monitoring, it is necessary to attempt new approaches using other dyes such as methylene blue. Using currently used dyes that can provide strong visibility could be helpful to be close to practical use.

CONCLUSION

In this study, a ^{99m}Tc-MSA-NBB conjugate was developed as a multimodal imaging agent for SLN mapping that can be assessed by visual monitoring, fluorescence imaging, and SPECT/CT. It was demonstrated that the ^{99m}Tc-MSA-NBB conjugate is quickly bound to, and accumulated in popliteal LN after footpad injection. Visual assessment was available with convenience and fluorescence imaging demonstrated high sensitivity. SPECT/CT allowed accurate quantification and localization of SLN before surgery. Thus, ^{99m}Tc-MSA-NBB conjugate has a great potential to be used as a multimodal imaging agent for preoperative and intraoperative SLN mapping.

REFERENCES

1. Morton DL, Wen DR, Wong JH, et al. Technical details of intraoperative lymphatic mapping for early stage melanoma. *Arch Surg.* 1992;127:392-399.

2. Giuliano AE, Kirgan DM, Guenther JM, DL M. Lymphatic mapping and sentinel lymphadenectomy for breast cancer. *Ann Surg Oncol.* 1994;220:391-398.

3. Pijpers R, Collet GJ, Meijer S, OS H. The impact of dynamic lymphoscintigraphy and gamma probe guidance on sentinel node biopsy in melanoma. *Eur J Nucl Med.* 1995;22:1238-1241.

4. Mariani G, Moresco L, Villa G, et al. Radioguided sentinel lymph node biopsy in breast cancer surgery. *J Nucl Med.* 2001;42:1198-1215.

5. Mariani G, Gipponi M, Moresco L, et al. Radioguided sentinel lymph node biopsy in malignant cutaneous melanoma. *J Nucl Med.* 2002;43:811-827.

6. Mirzaei S, Rodrigues M, Hoffmann B, et al. Sentinel lymph node detection with large human serum albumin colloid particles in breast cancer. *Eur J Nucl Med Mol Imaging.* 2003;30:874-878.

7. Uren RF, Howman-Giles R, JF T. Patterns of lymphatic drainage from the skin in patients with melanoma. *J Nucl Med.* 2003;44:570-582.

8. Dauphine CE, Khalkhali I, Vargas MP, Isaac NM, Haukoos J, Vargas HI. Intraoperative injection of technetium-99m sulfur colloid is effective in the

detection of sentinel lymph nodes in breast cancer. *Am J Surg.* 2006;192:423-426.

9. Flett MM, Going JJ, Stanton PD, TG C. Sentinel node localization in patients with breast cancer. *Br J Surg.* 1998;85:991-993.

10. Ka K. Sentinel lymph node mapping in breast cancer using subareolar injection of blue dye. *J Am Coll Surg.* 1999;189:539-545.

11. Mathelin C, Croce S, Brasse D, et al. Methylene blue dye, an accurate dye for sentinel lymph node identification in early breast cancer. *Anticancer Res.* 2009;29:4119-4125.

12. Bakhtiar N, Jaleel F, Moosa FA, Qureshi NA, Jawaid M. Sentinel lymph node identification by blue dye in patients with breast carcinoma. *Pak J Med Sci.* 2016;32:448-451.

13. Alex JC, Weaver DL, Fairbank JT, Rankin BS, DN K. Gamma-probe-guided lymph node localization in malignant melanoma. *Surg Oncol.* 1993;2:303-308.

14. Krag DN, Weaver DL, Alex JC, JT F. Surgical resection and radiolocalization of the sentinel lymph node in breast cancer using a gamma probe. *Surg Oncol.* 1993;2:335-339.

15. Pijpers R, Meijer S, Hoekstra OS, et al. Impact of lymphoscintigraphy on sentinel node identification with technetium-99m-colloidal albumin in breast cancer. *J Nucl Med.* 1997;38:366-368.

16. Gulec SA, Moffat FL, Carroll RG, et al. Sentinel lymph node localization in early breast cancer. *J Nucl Med.* 1998;39:1388-1393.

17. Jeong JM, Hong MK, Kim YJ, et al. Development of ^{99m}Tc-neomannosyl human serum albumin (^{99m}Tc-MSA) as a novel receptor binding agent for sentinel lymph node imaging. *Nucl Med Commun.* 2004;25:1211-1217.

18. Kim S, Jeong JM, Hong MK, et al. Differential receptor targeting of liver cells using ^{99m}Tc-neoglycosylated human serum albumins. *Arch Pharm Res.* 2008;31:60-66.

19. Choi JY, Jeong JM, Yoo BC, et al. Development of ^{68}Ga-labeled mannosylated human serum albumin (MSA) as a lymph node imaging agent for positron emission tomography. *Nucl Med Biol.* 2011;38:371-379.

20. Kim HK, Kim S, Park JJ, Jeong JM, Mok YJ, Choi YH. Sentinel node identification using technetium-99m neomannosyl human serum albumin in esophageal cancer. *Ann Thorac Surg.* 2011;91:1517-1522.

21. Kim HK, Kim S, Sung HK, Lee YS, Jeong JM, Choi YH. Comparison between preoperative versus intraoperative injection of technetium-99m neomannosyl human serum albumin for sentinel lymph node identification in early stage lung cancer. *Ann Surg Oncol.* 2012;19:1343-1349.

22. Kim EJ, Kim S, Seo HS, et al. Novel PET imaging of atherosclerosis with ^{68}Ga-labeled NOTA-neomannosylated human serum albumin. *J Nucl Med.* 2016;57:1792-1797.

23. Kim HK, Quan YH, Oh Y, et al. Macrophage-targeted indocyanine green-neomannosyl human serum albumin for intraoperative sentinel lymph node mapping in porcine esophagus. *Ann Thorac Surg.* 2016;102:1149-1155.

24. Lee SP, Im HJ, Kang S, et al. Noninvasive imaging of myocardial inflammation in myocarditis using ^{68}Ga-tagged mannosylated human serum albumin positron emission tomography. *Theranostics.* 2017;7:413-424.

25. Vera DR, Wisner ER, RC S. Sentinel node imaging via a nonparticulate receptor-binding radiotracer. *J Nucl Med.* 1997;38:530-535.

26. Vera DR, Wallace AM, CK H. [^{99m}Tc]MAG_3-mannosyl-dextran: a receptor-binding radiopharmaceutical for sentinel node detection. *Nucl Med Biol.* 2001;28:493-498.

27. Vera DR, Wallace AM, Hoh CK, RF M. A synthetic macromolecule for sentinel node detection ^{99m}Tc-DTPA-mannosyl-dextran. *J Nucl Med.* 2001;42:951-959.

28. Ellner SJ, Hoh CK, Vera DR, Darrah DD, Schulteis G, AM W. Dose-dependent biodistribution of [^{99m}Tc]DTPA-mannosyl-dextran for breast cancer sentinel lymph node mapping. *Nucl Med Biol.* 2003;30:805-810.

29. Hoh CK, Wallace AM, Vera DR. Preclinical studies of [^{99m}Tc]DTPA-mannosyl-dextran. *Nucl Med Biol.* 2003;30:457-464.

30. Emerson DK, Limmer KK, Hall DJ, et al. A receptor-targeted fluorescent

radiopharmaceutical for multireporter sentinel lymph node imaging. *Radiology.* 2012;265:186-193.

31. Liss MA, Farshchi-Heydari S, Qin Z, et al. Preclinical evaluation of robotic-assisted sentinel lymph node fluorescence imaging. *J Nucl Med.* 2014;55:1552-1556.

32. Liss MA, Stroup SP, Qin Z, et al. Robotic-assisted fluorescence sentinel lymph node mapping using multimodal image guidance in an animal model. *Urology.* 2014;84:982.e989-928.914.

33. Qin Z, Hoh CK, Hall DJ, Vera DR. A tri-modal molecular imaging agent for sentinel lymph node mapping. *Nucl Med Biol.* 2015;42:917-922.

34. Lee HJ, Barback CV, Hoh CK, et al. Fluorescence-based molecular imaging of porcine urinary bladder dentinel lymph nodes. *J Nucl Med.* 2017;58:547-553.

35. Pesek S, Ashikaga T, Krag LE, Krag D. The false-negative rate of sentinel node biopsy in patients with breast cancer: a meta-analysis. *World J Surg.* 2012;36:2239-2251.

36. Sadeghi R, Alesheikh G, Zakavi SR, et al. Added value of blue dye injection in sentinel node biopsy of breast cancer patients: do all patients need blue dye? *Int J Surg.* 2014;12:325-328.

37. Albertini JJ, Lyman GH, Cox C, et al. Lymphatic mapping and sentinel node biopsy in the patient with breast cancer. *JAMA.* 1996;276:1818-1822.

38. O'Hea BJ, Hill AD, El-Shirbiny AM, et al. Sentinel lymph node biopsy in breast cancer: initial experience at Memorial Sloan-Kettering Cancer Center. *J Am Coll Surg.* 1998;186:423-427.

39. Linehan DC, Hill AD, Akhurst T, et al. Intradermal radiocolloid and intraparenchymal blue dye injection optimize sentinel node identification in breast cancer patients. *Ann Surg Oncol.* 1999;6:450-454.

40. Boolbol SK, Fey JV, Borgen PI, et al. Intradermal isotope injection a highly accurate method of lymphatic mapping in breast carcinoma. *Ann Surg Oncol.* 2001;8:20-24.

41. Layeeque R, Kepple J, Henry-Tillman RS, et al. Intraoperative subareolar radioisotope injection for immediate sentinel lymph node biopsy. *Ann Surg.* 2004;239:841-848.

42. Radovanovic Z, Golubovic A, Plzak A, Stojiljkovic B, Radovanovic D. Blue dye versus combined blue dye-radioactive tracer technique in detection of sentinel lymph node in breast cancer. *Eur J Surg Oncol.* 2004;30:913-917.

43. Rodier JF, Velten M, Wilt M, et al. Prospective multicentric randomized study comparing periareolar and peritumoral injection of radiotracer and blue dye for the detection of sentinel lymph node in breast sparing procedures: FRANSENODE trial. *J Clin Oncol.* 2007;25:3664-3669.

44. Tellier F, Poulet P, Ghnassia JP, Wilt M, Weitbruch D, Rodier JF. A new optical probe for the detection of the sentinel lymph node using patent blue V dye in breast cancer: a preliminary study. *Mol Clin Oncol.*

2013;1:143-147.

45. He PS, Li F, Li GH, Guo C, Chen TJ. The combination of blue dye and radioisotope versus radioisotope alone during sentinel lymph node biopsy for breast cancer: a systematic review. *BMC Cancer.* 2016;16:107.

46. Sutton R, Tsopelas C, Kollias J, Chatterton BE, Coventry BJ. Sentinel node biopsy and lymphoscintigraphy with a technetium 99m labeled blue dye in a rabbit model. *Surgery.* 2002;131:44-49.

47. Tsopelas C, Bellon M, Bevington E, Kollias J, Shibli S, Chatterton BE. Lymphatic mapping with ^{99m}Tc-evans blue dye in sheep. *Ann Nucl Med.* 2008;22:777-785.

48. Zhang W, Wu P, Li F, Tong G, Chen X, Zhu Z. Potential applications of using ^{68}Ga-evans blue PET/CT in the evaluation of lymphatic disorder: preliminary observations. *Clin Nucl Med.* 2016;41:302-308.

49. Tsopelas C, R S. Why certain dyes are useful for localizing the sentinel lymph node. *J Nucl Med.* 2002;43:1377-1382.

50. Rawson R. The binding of T-1824 and structurally related diazo dyes by the plasma proteins. *Am J Physiol.* 1943;138:708-717.

51. FL R. Direct spectrophotometric determination of albumin in human serum. *Clin Chem.* 1965:478-487.

52. Miyada DS, Baysinger V, Notrica S, RM N. Albumin quantitation by dye

binding and salt fractionation techniques. *Clin Chem.* 1972;18:52-56.

53. Pinnell AE, BE N. New automated dye-binding method for serum albumin determination with bromcresol purple. *Clin Chem.* 1978;24:80-86.

54. RL W. A comparison of dye binding methods for albumin determination: the effects of abnormal sera, reaction times, acute phase reactants and albumin standards. *Clin Biochem.* 1983;16:178-181.

55. PG H. The measurement of albumin in serum and plasma. *Ann Clin Biochem.* 1985;22:565-578.

56. McGinlay JM, RB P. Serum albumin by dye-binding: bromocresol green or bromocresol purple? The case for conservatism. *Ann Clin Biochem.* 1988;25:417-421.

57. Dumas BT, Watson WA, HG B. Albumin standards and the measurement of serum albumin with bromcresol green. *Clin Chim Acta.* 1997;3:21-30.

58. Surasi DS, O'Malley J, Bhambhvani P. ^{99m}Tc-tilmanocept: a novel molecular agent for lymphatic mapping and sentinel lymph node localization. *J Nucl Med Technol.* 2015;43:87-91.

59. He XM, DC C. Atomic structure and chemistry of human serum albumin. *Nature.* 1992;16:209-215.

60. Popova TG, Espina V, Zhou W, Mueller C, Liotta L, Popov SG. Whole proteome analysis of mouse lymph nodes in cutaneous anthrax. *PLoS One.*

2014;9:e110873.

61. Troyan SL, Kianzad V, Gibbs-Strauss SL, et al. The FLARE intraoperative near-infrared fluorescence imaging system: a first-in-human clinical trial in breast cancer sentinel lymph node mapping. *Ann Surg Oncol.* 2009;16:2943-2952.

62. Hutteman M, Mieog JS, van der Vorst JR, et al. Randomized, double-blind comparison of indocyanine green with or without albumin premixing for near-infrared fluorescence imaging of sentinel lymph nodes in breast cancer patients. *Breast Cancer Res Treat.* 2011;127:163-170.

63. Oh Y, Lee YS, Quan YH, et al. Thoracoscopic color and fluorescence imaging system for sentinel lymph node mapping in porcine lung using indocyanine green-neomannosyl human serum albumin: intraoperative image-guided sentinel nodes navigation. *Ann Surg Oncol.* 2014;21:1182-1188.

국 문 초 록

^{99m}Tc-MSA와 염료 접합체를 사용한 감시림프절 맵핑용 다중모드영상제의 개발

이 지 연

서울대학교 대학원

의과학과 의과학전공

목적:

감시림프절은 원발성 종양으로부터 가장 가까이에 위치한 림프절이다. 유방암환자, 흑색종 암환자에서 감시림프절을 검출하는

것은 종양 병기를 평가하고, 수술 중 치료 결정을 하는데 중요한 역할을 한다. 현재 임상에서 청색 염료, 방사성 추적자, 방사성 추적자와 청색 염료 방법의 조합 그리고 방사성 동위원소가 표지된 청색 염료가 감시림프절 검출에 이용되고 있다. 그러나 이러한 방법에는 각각 한계가 있었다.

본 연구의 목표는 ^{99m}Tc이 표지된 MSA와 염료를 사용한 감시림프절 맵핑 영상제를 개발하는 것이었다. MSA와의 결합효율, 사이즈 배제 크로마토그래피를 이용한 고성능액체크로마토그래피 실험, 형광 모니터링과 같은 시험관 실험을 통해 다양한 염료를 테스트하였다. 그 중 MSA와 가장 높은 결합 효율을 보인 NBB가 선택되었고, 육안검사, 형광 이미징 그리고 단일 광자 방출 컴퓨터 단층 촬영/컴퓨터 단층 촬영 (SPECT/CT)을 통해 감시림프절 맵핑 성능을 평가하였다.

방법:

육안검사는 8개의 염료를 사용하여 수행되었다. 1 mM의 염료 용액은 1 μmol의 염료를 1 mL의 증류수에 녹여 준비하였고, 증류수를 이용하여 0.25 mM에서 0.001 mM까지 연속 희석하였다. 준비된 염료 용액의 색상은 육안검사를 통해 비교되었다. MSA−염료 접합체의 분자흡광계수 (ε)를 구하기 위해, UV-VIS-NIR 스펙트럼 분석을

수행하였고 흡광도 (OD)는 350-850 nm의 Varioskan flash screening mode에서 측정되었다. MSA와 다양한 염료간의 결합 효율은 반응 10분, 30분, 1시간, 2시간, 6시간 그리고 24시간 후 박층크로마토그래피를 통해 측정되었다. 박층크로마토그래피 플레이트는 Fujifilm LAS 3000를 이용하여 스캔하였고, multi-gauge 3.0를 이용하여 정량평가 하였다. 염료와 MSA 접합 전후의 크기를 확인하기 위하여 고성능액체크로마토그래피를 실행하였다. MSA-염료 접합체가 강한 형광 신호를 나타내는 파장대를 찾기 위해, 여기 420-780 nm, 방출 520-845 nm에서 형광 이미징 실험을 수행하였다. 감시림프절 맵핑을 위한 MSA-NBB 접합체의 성능을 평가하기 위해, MSA-NBB 접합체 혹은 NBB를 수컷 BALB/c 마우스 (총 12마리)에 투여 후 10분, 30분, 1시간 그리고 2시간에 육안 사진과 형광 이미지를 얻었다. SPECT/CT를 얻기 위해, MSA-NBB 접합체를 ^{99m}Tc으로 표지 하였고, 마우스(총 3마리) 좌측 발바닥에 피하 주사하였다. 약품 투여 10분, 30분, 1시간, 2시간 후 SPECT/CT를 얻었다.

결과:

육안 검사에서 모든 염료가 0.25 mM에서 명확한 색을 나타냈다. 희석된 일부 염료는 용액의 색을 확인하기 어려웠고, NBB, PBVF, NY, BR

그리고 EB는 0.004 mM의 낮은 농도에서도 잘 보였다. MSA-염료 접합체 각각을 정량화된 값으로 비교하기 위해, 흡광도 (OD)와 Beer-Lambert Law를 이용하여 분자흡광계수 (ε)를 계산하였다. MSA-PBVF 접합체는 141,481 M−1 · cm−1로 가장 높은 분자흡광계수를 나타내었으며, MSA-EB 접합체 (99259.3), MSA-ICG 접합체 (87037.0) 그리고 MSA-NBB 접합체 (62222.2)가 뒤를 이었다. 사이즈 배제 고성능액체크로마토그래피를 통해 MSA-염료 접합체가 단량체로 존재한다는 것을 확인하였다. 크로마토그램에서 준비된 모든 MSA-염료 접합체는 24시간 동안 안정하였고, 다른 응집체는 발견되지 않았다. 박층크로마토그래피결과는 MSA 농도와 결합 반응 시간이 증가됨에 따라 모든 염료와 MSA간의 결합 효율이 증가함을 보여주었다. 특히, 테스트된 모든 염료 중 NBB가 가장 적은 양의 MSA (2.5 mg)와 짧은 시간 (10분)내에 가장 높은 결합 친화력을 보였다. 결합 비율(mol/mol)은 NBB 0.7이 MSA 1과 결합된 것으로 계산되었다. 이러한 결과를 바탕으로, 생체 내 적용 실험을 위해 NBB가 선택되었다. MSA-NBB 접합체의 형광 신호는 여기 600 nm, 방출 670 nm에서 검출되었으며, 결합되지 않은 염료와 MSA의 형광 신호는 동일한 파장에서 검출되지 않았다. 육안검사에서, MSA-NBB 접합체가 NBB 단독으로 투여하였을 때 보다 모든 시간대에서 더 많은 슬와림프절 축적을 나타냈다. 약품 투여 10분 후 슬와림프절에 축적된 MSA-NBB 접합체와 NBB의 형광 세기는 각각

4.48±0.34 그리고 4.24±0.18 flux (10^8 p/s)이었다. 약품 투여 2시간 후 MSA-NBB 접합체의 슬와림프절 축적(4.81±1.24 flux (10^8 p/s))은 유지되었으나, NBB의 형광 세기는 빠르게 감소 (2.61±0.46 flux (10^8 p/s))하였다. 약품 투여 30분에서 2시간까지 MSA-NBB 접합체는 NBB 단독으로 투여하였을 때 보다 약 2배 높은 슬와림프절 축적을 보였다. SPECT/CT에서, ^{99m}Tc-MSA-NBB 접합체는 슬와림프절과 서혜부림프절에 높은 섭취를 보였다. 약품 투여 10분 후 슬와림프절과 서혜부림프절 각각에 섭취된 ^{99m}Tc-MSA-NBB 접합체의 SUV_{mean}은 13.08±2.33, 3.00±1.64이었고, 약품 투여 2시간 후에는 17.83±5.85, 4.99±3.44이었다. SPECT/CT 결과를 통해, 모든 시간대에서 ^{99m}Tc-MSA-NBB 접합체의 슬와림프절 축적이 서혜부림프절 축적보다 약 3.5배 높음을 확인하였다.

결론:

본 연구에서, ^{99m}Tc-MSA-NBB 접합체는 육안 검사, 형광 이미지 및 SPECT/CT를 위한 다중모드 감시림프절 맵핑 영상제로 개발되었다. 우리는 육안검사, 형광 이미지 그리고 SPECT/CT를 통해, 발바닥으로부터 가장 가까이에 위치한 슬와림프절 축적을 평가함으로써 ^{99m}Tc-MSA-NBB 접합체의 감시림프절 축적 능력을 평가하였다. 결과는

^{99m}Tc-MSA-NBB 접합체가 감시림프절에 빠르게 결합하고, 약품투여 2시간 후까지 감시림프절에 축적됨을 보여 주었다. 이러한 결과를 바탕으로, ^{99m}Tc-MSA-NBB 접합체가 임상에서 감시림프절 맵핑을 위해 사용될 가능성이 있음을 확인하였다.

주요어: MSA; 감시림프절 맵핑; 이미지 가이드 수술; 청색염료; 림프신티그라피; 다중모드

학번: 2014-30667